Meat Science 95 (2013) 940–957

Contents lists available at SciVerse ScienceDirect

Meat Science

journal homepage: www.elsevier.com/locate/meatsci

Modeling cooking of chicken meat in industrial tunnel ovens with the Flory–Rehner theory

R.G.M. van der Sman

Agrotechnology and Food Sciences Group, Wageningen University & Research, The Netherlands

ARTICLE INFO

Article history:
Received 3 February 2013
Received in revised form 25 March 2013
Accepted 25 March 2013

Keywords:
Water holding capacity
Cooking
Flory–Rehner theory

ABSTRACT

In this paper we present a numerical model describing the heat and mass transport during the cooking of chicken meat in industrial tunnels. The mass transport is driven by gradients in the swelling pressure, which is described by the Flory–Rehner theory, which relates to the water holding capacity (WHC). For cooking temperatures up to boiling point and practical relevant cooking times, the model renders good prediction of heat and mass transport and the total loss of moisture. We have shown that for cooking temperatures above boiling point, the model has to be extended with the dynamic growth of capillary water (drip) channels. Furthermore, we discuss that the Flory–Rehner theory provides the proper physical basis for describing the change of the WHC by a wide variety of factors like salt and pH.

1. Introduction

In a recent paper we have shown that the water holding capacity of meat can be described accurately by the Flory–Rehner theory (van der Sman, 2012b). The Flory–Rehner (FR) theory is commonly used to describe the swelling of synthetic polymer gels (Quesada-Pérez, Maroto-Centeno, Forcada, & Hidalgo-Alvarez, 2011). The theory is an extension of the Flory–Huggins theory (Flory, 1942), extended with an elastic term (Flory & Rehner, 1943). The FR theory gives the so-called swelling pressure as a function of solvent concentration. The FR theory equally applies to meat, if the effect of protein denaturation is accounted by a temperature dependency of the Flory–Huggins interaction parameter (van der Sman, 2012b). The water holding capacity is obtained from the FR theory via determining the equilibrium conditions. Under non-equilibrium conditions the FR theory renders the swelling pressure, whose gradient is the driving force of moisture transport during cooking (van der Sman, 2007a, 2007b). Recently, we have shown that the Flory–Rehner theory is also capable of describing the water holding capacity of other food materials, like mushrooms and vegetables (van der Sman, Voda, Khalloufi, & Paudel, submitted for publication).

At equilibrium the swelling pressure is zero, as the elastic contribution is balanced by the osmotic pressure (Quesada-Pérez et al., 2011). This last term is described by the Flory–Huggins-free-volume (FHFV) theory (van der Sman, 2012b; van der Sman et al., submitted for publication). The FHFV theory is yet another extension of the Flory–Huggins theory, which we have shown to describe the moisture sorption of a wide variety of (hydrophilic) food materials, like polysaccharides, sugars, polyols and proteins (van der Sman, 2012b, 2013; van der Sman & Meinders, 2011; van der Sman et al., submitted for publication). More, and more we are finding that with respect to moisture transport food materials are showing a similar behavior, which can be described by universal theories. This does not only hold for equilibrium properties like water activity, but also to the dynamics of moisture transport, i.e., the Fickian diffusion coefficient (Jin, van der Sman, & van Boxtel, 2011; van der Sman & Meinders, 2013). These recent studies are part of our quest, where we intend to show that soft matter physics applies to food materials, and profound insights can be gained via this approach (van der Sman & van der Goot, 2009) — as shown in a recent Faraday discussion on that subject (van der Sman, 2012a).

This quest has been initiated by our prior research on meat cooking, where we have focused on the cooking of beef (van der Sman, 2007a, 2007b). Here, we report on the application of the soft matter approach to cooking of chicken filet meat in industrial tunnels, using an extension of our previous numerical model. In these cooking tunnels one has good control over the air temperature, its dew point and airflow velocity, which are means to control the final moisture content of the cooked chicken filet. For some applications the air temperature is raised above boiling point, to induce crust formation on the chicken filet. Crust formation requires that water activity of the surface of the meat becomes significantly below unity. To incorporate this phenomenon into our model, we have to extend it with internal evaporation. Like in our previous model, we will follow the porous media approach, as propagated by Datta and coworkers (Datta, 2007; Dhall & Datta, 2011; Ni, Datta, & Torrance, 1999; Zhang & Datta, 2004).

To model intensive heating processes like frying and baking of food, Datta has used the volume-averaging approach, as pioneered by Whitaker

E-mail address: ruud.vandersman@wur.nl.

0309-1740/$ – see front matter © 2013 Elsevier Ltd. All rights reserved.
http://dx.doi.org/10.1016/j.meatsci.2013.03.027

to describe multiphase transport in porous media (Quintard & Whitaker, 1993; Whitaker, 1983). It is shown that during intensive heating pressure driven transport gives a very significant contribution to the total moisture transport (Ni et al., 1999; Zhang & Datta, 2006). The gradient of this pressure is inserted in Darcy's law, which is commonly used to describe liquid transport in porous media. Prior to the publications of Datta, one finds in literature of drying and intensive heating only phenomenological models (Vagenas, Marinos-Kouris, & Saravacos, 1990; Waananen, Litchfield, & Okos, 1993). There, multiphase transport is lumped into effective moisture diffusion processes — which does not have any physical basis. In the frying models of Singh and coworkers (Farkas, Singh, & Rumsey, 1996), one is aware of the approach of Whitaker, and uses it for gas transport in the crust region, but still they describe liquid moisture transport by a diffusion process. The more physics-based approach of Datta is gradually being followed by more and more food researchers (Dinčov, Parrott, & Pericleous, 2004; Feyissa, Gernaey, & Adler-Nissen, 2013; Huang, Yang, & Lee, 2013; Mir-Bel, Oria, & Salvador, 2009; Rajkumar, Moreira, & Barrufet, 2003; van der Sman, 2007a, 2007b; Wallach, Troygot, & Saguy, 2011; Weerts, Lian, & Martin, 2004, 2006).

In a recent paper Datta has addressed the cooking of meat, where the meat is initially in the frozen state (Dhall, Halder, & Datta, 2012). The meat product they considered is hamburger, and consequently they have taken fat transport also into account. Furthermore, they have also considered internal evaporation. The liquid transport is assumed to be driven by gradients in the capillary pressure, whereas we have considered the swelling pressure as the driving force. The capillary pressure is assumed to be a function of temperature and moisture content. The mass flux due to the gradient in capillary pressure is expanded, as is rewritten in two terms, linear in the gradient of the temperature and the gradient of the moisture content — similar to the phenomenological model of Luikov (1966). In our first paper we have shown that the Luikov model is mathematically equivalent to our model (van der Sman, 2007a, 2007b), and thus also to the recent model of Datta (Dhall et al., 2012). However, the models differ in the physics governing the moisture transport. We will explicitly distinguish three phases of water, the solid (intracellular) phases of meat fibers, the liquid and gas phases in the pores of the extracellular space. The water in each of the phases will be characterized by its own thermodynamic constitutive relation, which can be rewritten as a pressure. The swelling pressure relates to the solid phase, while the capillary pressure relates to the liquid phase. We will assume local equilibrium, meaning that the capillary pressure and swelling pressure are identical. Hence, this contributes to the mathematical equivalency of our model and Datta's model. In fact, the models differ only in the thermodynamic constitutive relations for the pressure. More discussion on the differences between the two models can be found in a recent discussion paper we have written together with Datta, van der Sman, Gulati, and Warning (2012).

A number of other papers have followed our approach with the swelling pressure (or its approximation by the "water demand") as the driving force (Aliño, Grau, Fernández-Sánchez, Arnold, & Barat, 2010; Feyissa, 2011; Feyissa et al., 2013; Goñi & Salvadori, 2010). A device for measuring the swelling pressure of (brined) meat has been developed (Aliño et al., 2010). Our modeling approach has been implemented in Comsol in Ref. Feyissa et al. (2013), and is combined with a moving mesh to account for the shrinkage of the meat (Feyissa, 2011). To our knowledge, this is the only model, which has implemented shrinkage during meat cooking, using a swelling pressure or water demand as a driving force for liquid transport. It is correlated to the experimentally observed shrinkage of a rectangular piece of meat during cooking. They account for temperature dependency of elasticity. Diffusion is superimposed on this. Proper modeling of shrinkage of irregular shaped meat like chicken filet requires knowledge of the elasticity of meat, which is only in its infancy (Dhall & Datta, 2011; Lepetit, 1989, 2007, 2008).

Our model on the moisture migration during the cooking of meat is a clear example of a model based on pressure driven flow (Datta, 2007; Perré & Turner, 1999). Most earlier models are based on a generalized Fickian diffusion model, with the gradient in moisture content (on dry basis) as the driving force. It is more and more recognized that the diffusion model cannot explain all phenomenons occurring during moisture migration in food and gels (Datta, 2007; Dhall & Datta, 2011; Okuzono & Doi, 2008; Wählby & Skjöldebrand, 2001). Our swelling pressure driven flow model can explain the migration of moisture towards the center during the cooking of meat in the initial stage of cooking (van der Sman, 2007a, 2007b; Wählby & Skjöldebrand, 2001). A similar phenomenon is experimentally observed during drying of broccolli and apple, which is explained by pressure driven flow (Aregawi et al., 2012; Jin, van Boxtel, & van der Sman, 2012). In this paper we will investigate the applicability of such a model to cooking and roasting of chicken filet.

We have organized this paper as follows. First, we present the Flory–Rehner and Flory–Huggins-free-volume theories, which describe the thermodynamics meat, i.e., swelling pressure and water activity. The theories are described in more detail in previous papers, but we would like to keep this paper self-contained. Subsequently, we present the numerical model as based on the porous media approach of Datta, but with the swelling pressure as the driving force for liquid transport. Next, we present the experiments performed to investigate the cooking of chicken filet in industrial ovens. The experimental data will be compared to the results of the computer simulations. We conclude with an extensive discussion on the obtained results, our modeling approach, and the prospects of the Flory–Rehner theory with respect to explaining water holding capacity.

2. Theory

2.1. Flory–Rehner theory and water holding capacity

We briefly describe here the thermodynamics of meat as follows from the FR theory, with details given in our earlier paper (van der Sman, 2012b). Strictly speaking, the FR theory only applies to the water absorbed by the food matrix (the intracellular space of meat fibers). However, as explained below, we assume that the contribution of capillary water in the extracellular space is negligible in the total water holding capacity. The FR theory describes the state of materials in terms of a swelling pressure Π_{sw}. The terminology of swelling pressure is taken from the field of swelling hydrogels, where the Flory–Rehner theory is traditionally applied (McKenna & Horkay, 1994). Although meat shrinks during cooking, we still adhere to the common terminology of swelling pressure.

The swelling pressure has three contributions:

$$\Pi_{sw} = \Pi_{mix} + \Pi_{ion} + \Pi_{elas}. \quad (1)$$

Its contributions are due to a) mixing of proteins and water Π_{mix}, b) the contribution of ions and polyelectrolytes Π_{ion}, and c) the elastic deformation of the crosslinked protein network Π_{elas}. The (mixing) osmotic pressure, Pi_{mix}, is computed from the composition of the food following the Flory–Huggins theory, with temperature dependent Flory–Huggins interaction parameter. We have assumed that the interaction between polyelectrolytes and ions can be absorbed in an effective interaction parameter. Now, the ionic contribution, Π_{ion}, accounts only for natural occurring salts in meat, which is assumed to be an ideal solution. The osmotic pressure of the salt solution can be added to the total osmotic pressure. For the elastic contribution, Π_{elas}, we assume to follow the Rehner theory (van der Sman, 2012b).

Below, we have given explicit formulations of each contribution in the Flory–Rehner:

$$\begin{aligned}\Pi_{\text{mix}} &= +\frac{RT}{v_w}\left[\ln(1-\phi)+\phi+\chi\phi^2\right]\\ \Pi_{\text{el}} &= -\frac{RT}{v_w}N_c\phi_0\left[\frac{1}{2}(\phi/\phi_0)-(\phi/\phi_0)^{1/3}\right]\\ \Pi_{\text{ion}} &= +\frac{RT}{v_w}\ln\left(a_{w,\text{ion}}\right).\end{aligned} \tag{2}$$

R is the universal gas constant, T the absolute temperature (given in Kelvin), v_w is the molar volume of water, ϕ is the volume fraction of the polymer, χ is the Flory–Huggins interaction parameter, N_c is the average number of monomers between crosslinks, ϕ_0 is the volume fraction of polymer at crosslinking, and $a_{w,\text{ion}}$ is the water activity due to the added ions. The elastic modulus of the gel E_0 at $\phi=\phi_0$ can be related to the following parameters:

$$E_0 = \frac{RT}{2v_w}N_c\phi_0. \tag{3}$$

One can view E_0 as a fitting parameter.

We compute $a_{w,\text{ion}}$ with Raoult's law:

$$a_{w,\text{ion}} = \frac{y_w/M_w}{y_w/M_w+\eta_{\text{ash}}y_{\text{ash}}/M_{\text{ash}}}. \tag{4}$$

Here y_w is the mass fraction of water, M_w is the molar weight of water, η_{ash} is the dissociation constant for the ions, y_{ash} is the mass fraction of the ions, and $M_{\text{ash}}=47$ g/mol is their effective molar weight (van der Sman & Boer, 2005; van der Sman, 2012b). Upon solution in water salts dissociated in multiple ions, the number of dissociation ions per salt molecule is counted by $\eta_{\text{ash}}=2$.

2.2. Flory–Huggins-free-volume theory

The above given Flory–Huggins expression for the osmotic pressure only holds when the meat is in the rubbery state. If the meat enters the glassy state, the osmotic pressure is computed using the Flory–Huggins-free-volume (FHFV) theory (van der Sman, 2012b). Furthermore, the Flory–Huggins interaction parameter is temperature dependent due to protein denaturation. We have validated this theory against sorption isotherms, which gives the water activity a_w as a function of moisture content. The relation between osmotic pressure and water activity is: $\Pi_{\text{mix}}v_w = RTln(a_{w,\text{mix}})$. Below, we describe the FHFV theory in terms of the water activity (with ϕ_w the volume fraction of water):

$$\ln\left(a_{w,\text{mix}}\right) = \ln(\phi_w)+(1-\phi_w)+\chi_p(T,\phi_w)(1-\phi_w)^2+F_{\text{FV}}. \tag{5}$$

F_{FV} is the free volume contribution due to structural relaxation in the glassy state, as developed by Vrentas and Vrentas.

The interaction parameter of proteins is composition and temperature dependent:

$$\chi_p(T,\phi) = \chi_{p,1}(T)-\left(\chi_{p,1}(T)-\chi_{p,0}\right)\phi_w^2 \tag{6}$$

with $\chi_{p,1}$ the interaction parameter of the dry polymer, and $\chi_{p,0}=0.5$ the interaction parameter of a fully hydrated polymer.

The free volume contribution F_{FV} is computed similar to earlier papers (He, Fowler, & Toner, 2006; van der Sman, 2012b, 2013; van der Sman & Meinders, 2011):

$$F_{\text{FV}} = -M_w y_w^2\frac{\Delta C_{p,S}}{RT}\frac{dT_g}{dy_w}\frac{T-T_g}{T_g}. \tag{7}$$

If the food is in the rubbery state, if $T>T_g$, the contribution of the structural relaxation is assumed to be zero: $F_{\text{FV}}=0$. In the above equation, M_w is the molar weight of water, y_w is the mass fraction of water, $\Delta C_{p,S}$ is the change in heat capacity at the glass transition, and T_g is the glass transition temperature, which depends on the moisture content y_w. Earlier, we have shown that for biopolymers, and sugars $\Delta C_{p,S}$ has the universal value of $\Delta C_{p,S}=0.42$ kJ/kg · K (van der Sman, 2012b, 2013; van der Sman & Meinders, 2011). We assume that the ashes present in the meat do not influence T_g. Furthermore, we note that F_{FV} will not influence the WHC, as the meat is then in the rubbery state, and $F_{\text{FV}}=0$.

As said, the water holding capacity of meat is obtained at equilibrium conditions, without any external mechanical load — where $\Pi_{\text{sw}}=0$. In Appendix A we have repeated the comparison of the experimental and theoretical values of the water holding capacity for various types of meat, amongst which is chicken meat (van der Sman, 2012b).

2.3. Moisture transport

During intensive heating of meat, water can be in various phases (Datta et al., 2012). One can distinguish the following phases: 1) the intracellular water, absorbed by the solid phase of meat proteins, 1) the extracellular (capillary) water in the pores between the meat fibers, and 3) water vapor, if internal evaporation occurs. Internal evaporation occurs, if a) the local temperature is at boiling temperature (vapor bubbles are formed via heterogeneous nucleation), or b) the capillary water at the surface has evaporated and an evaporation front is moving into the meat. In case of b) water vapor is generated at the interface of the vapor phase and the capillary water phase. There will be a diffuse transition zone between the dry crust and the wet core, where vapor phase and liquid water phase coexist. The capillary water phase is then a liquid film around the meat fibers, with curved menisci in the corners of the pores. We have depicted the different water phases schematically in Fig. 1.

We will assume local thermodynamic equilibrium between all phases of water. Each phase will be characterized by a pressure. The gas phase is characterized by the gas pressure p_{gas}, which incorporates the partial water vapor pressure p_{vap}. The capillary water is characterized by a capillary pressure $p_{\text{cap}}=p_{\text{liq}}-p_{\text{gas}}$, while the solid phase is characterized by the swelling pressure, Π_{sw}. We will assume local equilibrium, and consequently the swelling pressure is equal to the capillary pressure.

Here, we must make a note on the misconception that in liquid pressure in the intracellular phase is a capillary pressure, and that it follows the Young–Laplace law. However, the spacing between protein fibers is

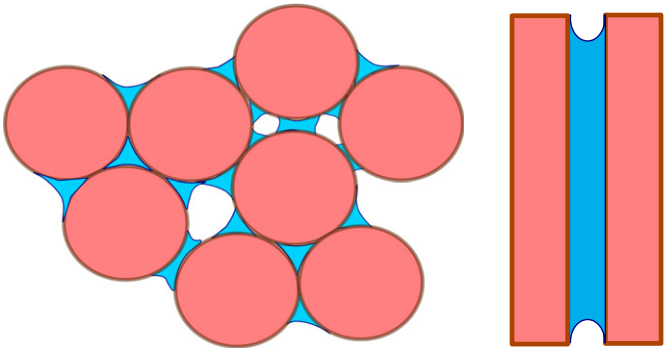

Fig. 1. Schematic representation of different water phases in meat. Pink regions indicate the protein fibers with absorbed water, forming roughly a hexagonal lattice, with capillary water filling the extracellular pores (blue regions). Capillary water has curved interfaces if it bounds the gas phase (white), which contains water vapor. We have depicted two different cross sections.

in the nanometer range, and consequently also the disjoining pressures contribute to the liquid pressure (Elliott & Hodson, 1999; Puolanne & Halonen, 2010; Schreyer-Bennethum, 2012; Wang & Hong, 2010). The disjoining pressure arises due to van der Waals forces and electrostatic forces between the protein fibers, and their effect is effectively described by the Flory–Huggins interaction parameter. In the 10–40 nanometer range the disjoining pressure (or equivalently the osmotic pressure) dominates over the capillary pressure, as computed from the Young–Laplace law. Due to the dependence of the disjoining pressure with the distance between the myofiber the liquid–gas interface in the intracellular space will be a thin flat film covering the myofibers.

Furthermore, it is pointless to make distinction between different kinds of water within the intracellular space. In the past one has often made a distinction between different waters — with naming them as hydration water, bound (unfreezable) water, and bulk water (Chou & Morr, 1979; Hills, Manning, & Ridge, 1996; Kneifel, Paquin, Abert, & Richard, 1991; Mathlouthi, 2001; Puolanne & Halonen, 2010). However, recent studies on the physics of protein hydration indicate that this is a highly oversimplified picture (Ball, 2008; Block, 2003; Halle, 2004; Wolfe, Bryant, & Koster, 2002). There is a whole continuum of water (dynamics), as its energy level changes with distance to the protein. The residence time of water in the hydration shell is only in the order of 100 ps, and the notion of different water layers is misleading (Ball, 2008). The effect of the continuum of energy levels can be coarse-grained with the Flory–Huggins or FVFH theory, where the interaction parameter is made dependent on the volume fraction (Baulin & Halperin, 2002; van der Sman, 2012b; van der Sman & Meinders, 2011). These theories are an approximation of the more fundamental Tanaka–Pincus–deGennes cluster model, which does account for different energy levels for hydrogen-bonding (Bekiranov, Bruinsma, & Pincus, 1997; De Gennes, 1991; Matsuyama & Tanaka, 1990). Hence, the protein/solute/water mixture in the intracellular space can be viewed as one single thermodynamic phase. The extracellular space must be treated as a separate thermodynamic phase, due to the absence of crosslinked protein matrix — similar as in microphase-separated gels (Leksrisompong, Lanier, & Foegeding, 2012).

The pressures for the different phases follow from the thermodynamic constraint for local equilibrium:

$$\exp\left(\frac{\Pi_{sw} v_w}{RT}\right) = \exp\left(\frac{p_{cap} v_w}{RT}\right) = a_{w,liq} = a_{w,gas} = \frac{p_{vap}}{p_{sat}(T)} \tag{8}$$

with the water activity for the liquid phase $a_{w,liq}$ following from the Kelvin relation. We note that the water activity of the gas phase equals the relative humidity by definition, which is the ratio of the partial water vapor pressure and the saturated vapor pressures (which is dependent on temperature).

If there is a gas phase present at temperatures below boiling temperature, there will also be an air (nitrogen) present in the gas phase. The partial vapor pressure will be below atmospheric pressure, but the total gas pressure is equal to atmospheric. Due to gradients in partial air pressure with the environment, air will diffuse in the gas phase, which is balanced by the diffusion of water vapor as the total gas pressure p_{gas} is presumed to be constant. At temperatures above boiling point, the gas phase consists only of water vapor. The gas pressure is equal to the vapor pressure given by the above equilibrium relation.

Because of the assumption of local equilibrium, we do not have to make a distinction between the various phases of water in our physical model. We have to state only a single mass balance for the total moisture content. However, below we will derive that from the individual mass balances for the three different phases. As the driving force for moisture transport we take the swelling pressure. The capillary pressure and water vapor pressure have only physical significance if a gas phase is present (with a coinciding curved interface between liquid and gas phases).

In our model we also neglect the effect of shrinkage of meat on the heat and mass transport. This is primarily done for the sake of keeping the complexity of the model to a moderate level. It is indeed questionable and negligible, as shrinkage can be very considerable during extensive cooking. However, taking this into account implies also taking the mechanical response of the meat into account, and a full poroelastic model has to be built, cf. (Dhall & Datta, 2011).

Each water phase will be described by the following densities: the amount of water absorbed by the solid phase n_b, the amount of capillary water n_w, and the amount of water vapor n_v. The capillary water and the gas phase occupy the pore space of the meat, which has a constant porosity of . The amount of pore space occupied by the capillary water is indicated by the saturation S_w, as is common in porous media literature. Their time evolution of the densities is governed by the following mass balances:

$$\begin{aligned} \partial_t n_b &= -\nabla\cdot\mathbf{j}_b - s_{bw} \\ \partial_t n_w &= -\nabla\cdot\mathbf{j}_w - s_{wv} + s_{bw} \\ \partial_t n_v &= -\nabla\cdot\mathbf{j}_v + s_{wv}. \end{aligned} \tag{9}$$

Here $\mathbf{j}_\alpha$ is the mass flux of phase α, and $s_{\alpha\beta}$ represents mass transfer from phase α to phase β (for example via evaporation). We assume that the absorbed moisture is always transported first to the capillary water phase, before it can evaporate.

The driving forces for the fluxes are the gradients in the pressures present in each phase. The flux laws will be written in terms of a generalized Darcy law:

$$j_b \sim \nabla\Pi_{sw};\ j_w \sim \nabla p_{liq};\ j_v \sim \nabla p_v. \tag{10}$$

We can take the assumption that $\nabla\, p_{liq} \gg \nabla\, p_{gas}$, and consequently $\nabla\, p_{liq} \approx \nabla\, p_{cap}$. In the experiments we have performed, we assume that the transport in the capillary water phase is dominant, as it offers the lower resistance than the solid phase, and has more capacity to transport moisture than the gas phase. However, during the experiments in regions near the skin of the chicken filets the meat becomes dry. Consequently, transport via the gas phase can become important relative to the capillary transport, due to the low water saturation in the pores — which makes the relative permeability for liquid very small.

The swelling pressure Π_{sw} is determined by the amount of water bound to the polymer n_b, and is given by the Flory–Rehner theory, as discussed above. Π_{sw} is given as a function of the volume fraction of absorbed water ϕ_w, which needs to be related to n_b via:

$$n_b = (1-\varepsilon)\phi_w\rho_w \tag{11}$$

where $1-\varepsilon$ is the relative fraction of the solid phase, of which the volume fraction ϕ_w is occupied by bound water, having a mass density of ρ_w.

The capillary pressure p_{cap} is determined by the amount of capillary water n_w. As is the custom in porous media science, we use a constitutive relation linking the capillary pressure to the liquid saturation of the pore space S_w. In Appendix A we discuss this constitutive relation, where we approximate meat as a hexagonal array of cylindrical fibers. The relation between saturation and the amount of capillary water is:

$$n_w = \varepsilon S_w \rho_w. \tag{12}$$

The vapor pressure p_v is related to the amount of vapor n_v via the ideal gas law:

$$n_v = \varepsilon(1-S_w)\frac{p_v M_w}{RT} \tag{13}$$

with M_w as the molar mass of water.

By the assumption of local equilibrium we can add the three mass balances, and the mass transfer functions $S_{\alpha\beta}$ will be canceled out. The total mass balance is for the total moisture content: $n = n_v + n_b + n_w$. After adding the individual mass balances, and using the assumption that the capillary transport is dominant, we obtain the total mass balance:

$$\partial_t n = -\nabla\cdot(\mathbf{j}_w + \mathbf{j}_v). \tag{14}$$

As stated above, we take the swelling pressure as the driving force for liquid transport. The related flux law is formulated in terms of Darcy's law:

$$\mathbf{j}_w = -\frac{\kappa_w}{\nu}\nabla\Pi_{\mathrm{sw}} \tag{15}$$

where ν is the kinematic viscosity of the plasma in the capillary phase, and κ_w is the so-called (liquid) permeability of the pore space. The viscosity ν will be different from water due to the fact that the plasma will contain sarcoplasmic proteins like myoglobin. The liquid permeability $\kappa_w = \kappa_0 k_{w,r}(S_w)$ is a function of the water saturation, with the dependency on saturation captured by the relative permeability $k_{w,r}$. The constitutive relation for $k_{w,r}$ is described in Appendix A.

If the gas phase is absent ($S_w = 1$) the flux law can be reformulated in terms of the 'water demand', the difference between the actual moisture content n and the water holding capacity $n^{\mathrm{eq}}(T)$. In this regime the permeability is assumed constant $\kappa_w = \kappa_0$. We used this formulation in our previous publications on meat cooking (van der Sman, 2007a, 2007b):

$$\mathbf{j}_w = -\frac{\kappa_0}{\nu}\nabla\Pi_{\mathrm{sw}} \approx \frac{\kappa_0}{\nu}\nabla\Sigma\left[n - n^{\mathrm{eq}}(T)\right]. \tag{16}$$

This approximation follows formally from a Landau expansion of the expression of the swelling pressure. Σ is some model constant, which now can be related to more fundamental parameters via the Landau expansion of Π_{sw}.

The flux for the water vapor transport (Ni et al., 1999):

$$\mathbf{j}_v = -\frac{k_{v,r}\kappa_0}{\nu_v}\nabla p_{\mathrm{gas}} - D_{v,\mathrm{eff}}\nabla n_v \tag{17}$$

where $k_{v,r}$ is the permeability of the gas phase, and is dependent on the water saturation S_w. Its constitutive relation is also discussed in Appendix A. ν_v is the viscosity of the gas phase, and can be obtained from physical tables. $D_{v,\mathrm{eff}}$ is the diffusivity of water vapor in the pore space, which is approximately equal to that in bulk gases, but is modulated by the porosity and tortuosity of the pore space.

The total gas pressure is given by:

$$\begin{array}{l} p_{\mathrm{gas}} = p_0 \ \text{ if } \ p_v < p_0 \\ p_{\mathrm{gas}} = p_v \ \text{ if } \ p_v \geq p_0 \end{array} \tag{18}$$

with p_0 the ambient pressure. Hence, below boiling point there is only water vapor transport via diffusion. Above boiling point there is convective transport, linear in the gradient of the gas pressure.

Under the assumption of no shrinkage, and that meat forms a hexagonal array of cylindrical fibers, the porosity is ≈ 0.1. Hence, we can safely assume that $n_b \gg n_w \gg n_v$. For computing the driving forces we assume that $n \approx n_b$. This approximation may even give an error in the liquid flux smaller than 10%, because the experimentally determined water holding capacity does not differentiate between capillary water and absorbed water. Hence, $n^{\mathrm{eq}} = n_b^{\mathrm{eq}} + n_w^{\mathrm{eq}}$. It is probably more accurate to use $n - n^{\mathrm{eq}}$ as the driving force.

If $n \geq n^{\mathrm{eq}}$ the pore space will always be completely filled with capillary water, and hence $S_w = 1$. Only if $n < n^{\mathrm{eq}}$, we have $S_w < 1$. Its value will be determined via the equilibrium relation $\Pi_{\mathrm{sw}} = p_{\mathrm{cap}}$. Because, we assume $n \approx n_b$, the swelling pressure is directly computed from the amount of moisture n, following from the Flory–Rehner theory Eq. (1). From the inverse relation of $p_{\mathrm{cap}}(S_w)$ we can compute the water saturation S_w. This quantity is only used to compute the permeabilities k_w and k_v.

The amount of water vapor is computed via $p_v = a_w p_{\mathrm{sat}}(T)$, with the water activity computed from the swelling pressure: $\Pi_{\mathrm{sw}} v_w = RT\ln(a_w)$. n_v is negligible compared to n_b, but the diffusive flux might become important at low values of the water saturation, where the water permeability becomes quite small — as indicated in Appendix A. Furthermore, the gas flux can also transport a significant amount of latent heat, which requires also knowledge of n_v.

2.4. Energy transport

For the formulation of the energy balance we follow the approach of Stanish for drying of hygroscopic porous media (Stanish, Schajer, & Kayihan, 2004). The energy content e of the meat is a function of temperature, and the amounts of water in the various states. Each phase has its own contribution to the total enthalpy of the system (h_α):

$$\begin{array}{l} e = n_b h_b(T) + n_w h_w(T) + n_v h_v(T) + n_p h_p(T) \\ h_b(T) = -r_{\mathrm{sorb}}(T) \\ h_w(T) = c_{p,w}(T - T_{\mathrm{ref}}) \\ h_v(T) = c_{p,v}(T - T_{\mathrm{ref}}) + r_{\mathrm{evap}}(T_{\mathrm{ref}}) \\ h_a(T) = c_{p,a}(T - T_{\mathrm{ref}}) \\ h_p(T) = c_{p,p}(T - T_{\mathrm{ref}}) \end{array} \tag{19}$$

where $n_p = (1-\epsilon)\rho_p$ is the amount of proteins, $c_{p,\alpha}$ the specific heat of phase α, r_{evap} the heat of evaporation of pure liquid water. The heat of sorption r_{sorb} follows from the Clausius–Clapeyron relation:

$$\frac{d\ln(a_w)}{dT} = \frac{r_{\mathrm{sorb}}}{RT^2}. \tag{20}$$

The balance equations for the energy read:

$$\partial_t e = -\nabla\cdot(h_w\mathbf{j}_w + h_v\mathbf{j}_v + \mathbf{q}).$$

with q the conductive heat flux. Note that the mass fluxes of liquid water and water vapor lead to convective energy fluxes, which transport the enthalpy contained in that water phase. The conductive heat flux follows from Fourier's law:

$$\mathbf{q} = -\lambda_m\nabla T. \tag{21}$$

The thermal conductivity λ_m is a tensorial quantity, which depends on the direction of the fibers and the liquid saturation S_w. Its constitutive relation is discussed in Appendix A.

2.5. Boundary conditions

For the energy balance we have a Neumann boundary condition for the heat flux:

$$\mathbf{q} = \alpha_{\mathrm{ext}}(T - T_0) \tag{22}$$

with α_{ext} the heat transfer coefficient, which is a function of the air flow velocity — as explained in Appendix A. T_0 is the air temperature.

For the evaporation at the boundary we have another Neumann boundary condition:

$$\mathbf{j_v} = \beta_{\mathrm{tot}}\left(n_v - n_{v,0}\right) \tag{23}$$

$n_{v,0}$ is the water vapor density in the air flow, often expressed in the dew point T_{dew}: $n_{v,0} = p_{\mathrm{sat}}(T_{\mathrm{dew}})M_w/RT_{\mathrm{dew}}$. The mass transfer

coefficient β_{tot} will have a different value for condensing conditions and for evaporating conditions.

If $n_v < n_{v,0}$ water vapor from the flowing air will condense on the surface of the meat. The condensation rate will be determined by the mass transfer coefficient of the boundary layer $\beta_{tot} = \beta_{ext}$. The condensed water is assumed to run off the meat, and will not contribute to the evaporative cooling effect. The external mass transfer coefficient β_{ext} is related to the external heat transfer coefficient α_{ext}, via the Lewis relation. It is further explained in Appendix A.

If $n_v > n_{v,0}$ moisture will evaporate from the meat. Next to the boundary layer, there is now an extra resistance to water vapor transport: the skin of the filet (the epimysium connective tissue), as characterized by another mass transfer coefficient β_{skin}. Under evaporation conditions the total mass transfer coefficient is:

$$1/\beta_{tot} = 1/\beta_{ext} + 1/\beta_{skin}. \tag{24}$$

To compute the convective moisture flux and the water vapor flux (if $p_v > p_0$) we use the following Dirichlet boundary conditions:

$$\pi_{sw} = 0; \quad p_{gas} = p_0. \tag{25}$$

We assume that expelled liquid moisture drips of the meat and does not contribute to the evaporative cooling of the meat, similar to the 'liquid pumping' boundary conditions as formulated by Ni et al. (1999).

2.6. Numerical solution method

The above energy and mass balance equations are discretized using the finite volume method. Central differencing is applied to the dissipative fluxes (linear with the gradient in pressure or temperature), while upwind differencing is applied to the convective fluxes (linear with the velocity). The balance equations are integrated in time using Euler forwarding, with a variable time step. The time step Δt is determined by the constraints that all local grids Fourier numbers $Fo^*_\alpha < 1/6$ and local Courant numbers $Cr_\alpha < 1/6$. The grid Fourier number and Courant number are defined as:

$$Fo^*_\alpha = \frac{\lambda_m \Delta x_\alpha}{\rho_m c_{p,m}} \tag{26}$$

$$Cr_\alpha = \frac{j_w \Delta t}{n \Delta x_\alpha} \tag{27}$$

with Δx_α the (local) grid spacing in the x_α (Cartesian) directions. $c_{p,m}$ is the heat capacity of the meat, obtained via weight averaging.

The driving force for moisture transport (the swelling pressure) and heat transport (temperature) are obtained from solving the constitutive equations and the condition of local equilibrium. Because of their implicit formulation they are solved iteratively, using the solution from the previous time step as an initial guess. In a similar way the driving forces at the surface have to be solved iteratively from the boundary conditions, the constitutive equations and the condition of local equilibrium.

Via a line scan, we have obtained a voxel representation of chicken filet, which is mapped to a rectangular grid of $20 \times 40 \times 20$ cells, with grid spacings $\Delta x = \Delta y = 4\Delta z$. For chicken filets having a mass equal to the reference mass $M_0 = 100$ g, the dimensions of the computation grid (bounding the chicken filet geometry) is $L_x = 8$ cm, $L_y = 16$ cm, and $L_z = 2$ cm. For chicken filets with different masses we will adjust the grid spacing, while keeping the number of grid cells constant ($20 \times 40 \times 20$).

In Fig. 2 we have displayed a 3D-plot of a chicken filet geometry. In the figure one can clearly observe the staircase representation of the geometry that we have used. This will of course give a slight error in the area for heat and mass transfer between filet and airflow, compared to an unstructured grid representation of the geometry. However, the implementation of an unstructured grid is much more involving than a rectangular structured grid. Commercial packages do not allow for moisture fluxes linear in a swelling pressure. Hence, we have developed our own code—which has been validated in our previous study. Errors in the heat and mass transfer at the surface of the chicken filets due to the staircase discretization will be absorbed in the (effective) external heat and mass transfer coefficients, which will be fitted.

3. Materials and methods

3.1. Water holding capacity

Experiments are performed via the standard procedure for determining cooking loss. The chicken filet is placed in a sealed plastic bag, and is submerged in a thermostated water bath for 24 h. The mass of the chicken filet is measured before and after the experiment with a scale (Mettler) having an accuracy of 0.1 g. Free water at the surface is removed with a non-sticking absorbent paper. The water holding capacity will be expressed in the mass fraction of water, and in the volume fraction of the polymer ϕ_p. The WHC data is fitted with the Flory–Rehner theory, together with data from other kinds of meat, as described in our previous paper (van der Sman, 2007b). The moisture content of the raw meat is determined via an oven test at 200 °C for 24 h.

3.2. Geometry discretization

To determine the geometry of a chicken filet, we have performed laser line scans (ScanTech) on three filets of different weights. The accuracy of the scanner is 0.1 mm. The scanned geometries are analyzed for self-similarity via rescaling of the axes. The rescaling is based on the assumption that all dimensions of the filet (length, width and height) scale as $L_\alpha \sim M^{1/3}$, with M as the mass of the filet. For all other analyzed chicken filets, which are subjected to tunnel cooking, we have determined the main dimensions (length, width and height) with a caliper. This is done before and after the cooking treatment. These lengths will be analyzed for their scaling with the total mass M.

3.3. Cooking experiments

A single chicken filet is placed in a linear industrial tunnel oven (Stork PMT). The filet is placed on a metal grid (as shown in Fig. 3),

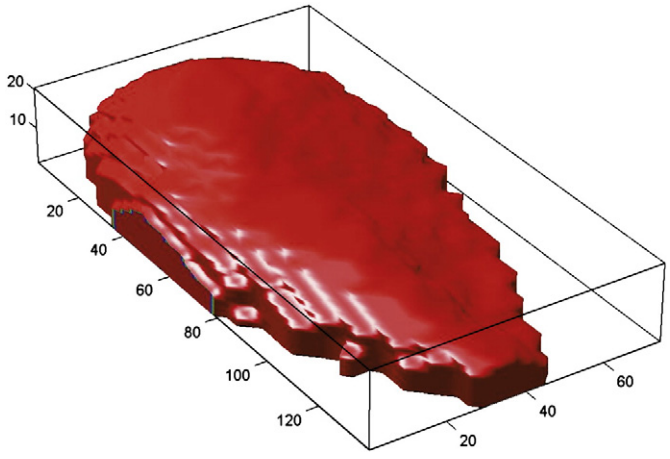

Fig. 2. 3D plot of the chicken filet geometry mapped onto a rectangular structured grid. Dimensions are in [mm], and correspond to a filet having a mass $M = M_0 = 100.0$ g.

which is held stationary in the middle of the tunnel. The meat on the grid is enclosed by a cubic box, with sides of 40 cm. The box has perforated plates in the front and the back side to obtain a uniform flow field approaching the piece of meat. In the series of experiments we have varied oven temperature (T_0), dew point (T_{dew}), air velocity (v_{air}), which are controlled via the set points of the industrial oven. Temperature is controlled within 0.5 °C, while the airflow velocity is controlled at 0.2 m/s. During each experiment we have measured core temperature, skin temperature with thermocouples, and the mass of the meat is measured with the Mettler scale before and after the cooking experiment. The duration of the experiment, the cooking time t_e, has ranged from 20 to 160 min depending on the settings of the oven. Table 1 shows the various chosen settings for the experiments, and includes the initial mass of the filet. At positive airflow velocities the airflow is from heat to tail, and negative airflow velocities indicate a reversal of airflow direction.

Temperature is recorded via needle thermocouples located at 1) the coldest point of the filet, which is beneath the point where the filet is the thickest, midway between top and bottom of the meat, and 2) 2 mm under the skin, at the point where the filet is the thickest (hence above the sensor measuring the coldest point). Temperature is recorded at either 1 or 5 second time interval. Accuracy of the thermocouple/data logger is 0.1 °C.

4. Results

4.1. Water holding capacity

The water holding capacity is obtained from experiment, to which a sigmoid function is fitted, following our previous paper (van der Sman, 2007a):

$$\frac{n^{eq}(T)}{\rho_m} = y_{w0} - \frac{\Delta y_w}{1 + A_\sigma \exp(-(T - T_\sigma)/\tau_\sigma)}. \quad (28)$$

Hence y_{w0} is the mass fraction of water in raw meat, and $y_{w1} = y_{w0} - \Delta y_w$ is the mass fraction of water in fully cooked meat. The oven test has shown that $y_{w0} = 0.79$. In Fig. 4 we have plotted the experimental data of the water holding capacity of chicken filet as a function of temperature, together with the fitted sigmoid function. Via regression we have obtained the following estimates of parameters: $\Delta y_w = 0.31$, $A_\sigma = 30.0$, $T_\sigma = 315$ K, $\tau_\sigma = 5.88$ K. These parameters are quite similar to those found for beef (van der Sman, 2007a).

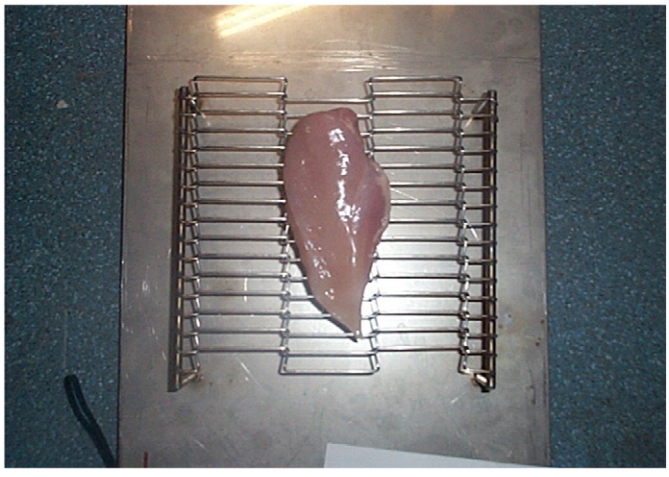

Fig. 3. Chicken filet placed on the metal grill, which is placed in the tunnel oven.

Table 1
Setup of the cooking experiments.

Index	T_{oven} [°C]	T_{dew} [°C]	v_{air}[m/s]	t_e [min]	Mass [g]
heat0a	45	45	10	160	192
heat1	45	45	10	80	164
heat5	60	60	10	60	174
heat7	60	60	10	40	142
heat10	80	70	10	40	196
heat12	80	70	10	20	156
final01	70	60	15	80	142
final02	70	65	7	120	138
final03	70	70	3	160	134
final04	70	60	−15	80	164
final05	70	65	−7	120	141
final06	70	70	−3	160	133
final07	55	55	15	80	135
final08	55	55	7	120	140
final09	55	55	3	160	138
final10	100	70	7	120	138
final11	100	70	3	120	135
boil3	150	70	10	80	156

4.2. Geometry discretization

A sample line scan is shown in Fig. 5. It is assumed that the filet lies more or less flat on the surface. Line scans are performed on filets having a mass of 104, 140 and 190 g. We compare their height maps, after performing a rescaling of coordinates. Here we take the filet with $M = M_0 = 104$ g as a reference. The rescaling of coordinates is as follows: $x_\alpha = x_\alpha(M/M_0)^{1/3}$, where x_α is the unscaled coordinate, as obtained from the line scan — with the center of gravity as the origin for the coordinate system. The height maps using rescaled coordinates are shown in Fig. 6 for all three scanned filets. As one can observe the height maps are quite isomorphic, and hence one can conclude that the proposed scaling of dimensions with mass holds $L_\alpha \sim M^{\frac{1}{3}}$.

The chicken geometry in the computer model will be constructed using the rescaled geometry of the filet for a mass of 100 g. The rescaling is fine tuned such that the volume times the density equals the total mass of 100 g at 0.1% accuracy. The density is computed from the assumption that chicken consists of 79% water and 21% proteins. In this fine tuning we have applied some Gaussian filtering to the voxel representation of the chicken filet, to remove voxels having more than 4 sides exposed to the air, to obtain a smooth surface.

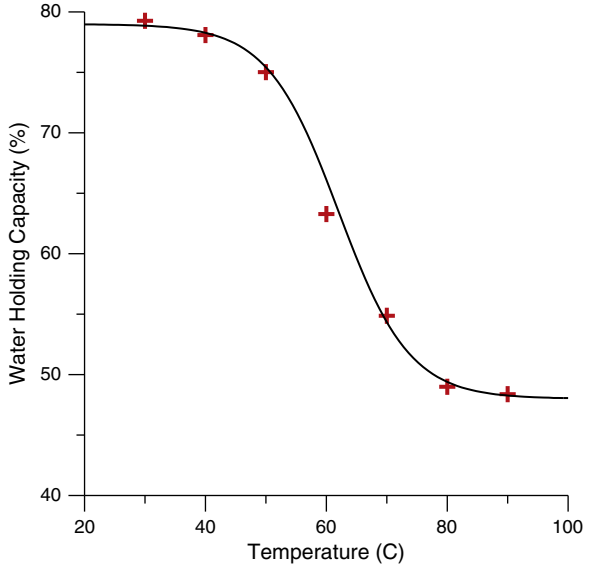

Fig. 4. Water holding capacity as a function of temperature T, as obtained from cooking loss experiments. The WHC is expressed in mass fraction of water y_w.

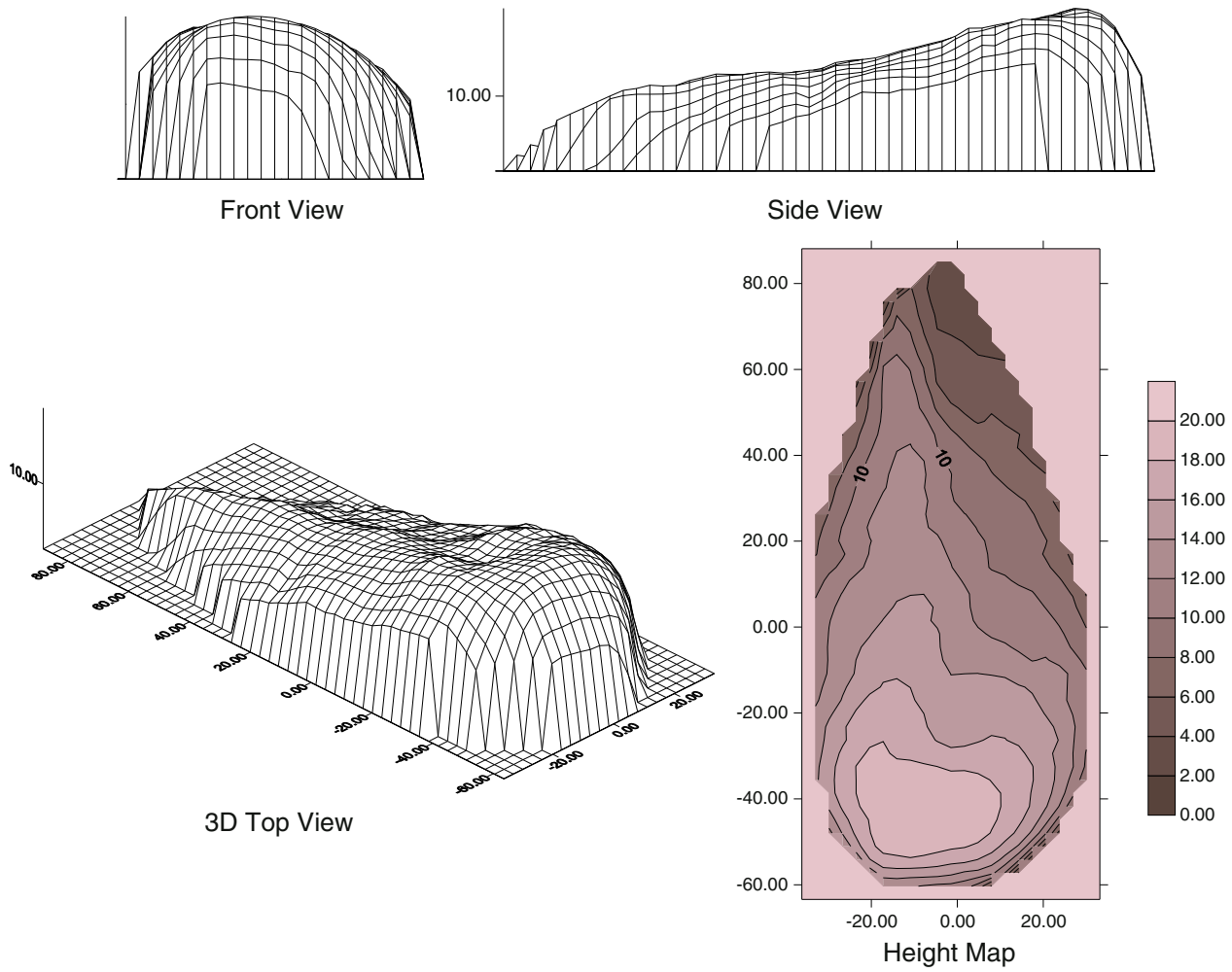

Fig. 5. Line scan of a chicken of 104 g. All dimensions are in [mm].

The above found that allometric scaling is checked against the dimensions of the chicken meat before and after the cooking experiment. The results are shown in Fig. 7. The allometric scaling rule is shown to be fitting to all data points, $L_\alpha \sim M^{\frac{1}{3}}$. However, there is a slight systematic deviation for the width of the filet between the scanned filets and the filets used for the cooking experiments (indicated with dotted and solid lines respectively in Fig. 7). Hence, the scanned chicken filets are not totally representative for the samples used in the cooking experiments. But, because the height is much smaller than the width, the heat and mass transport will mainly be determined by the height, and we assume the systematic deviation for the width of minor significance.

We note that also the dimensions of the cooked meat (mostly having uniform temperature at the end of experiment) follow the same allometric scaling rule, $L_\alpha \sim M^{\frac{1}{3}}$, albeit with different scaling constants. Via comparison of the scaling constants for the raw and cooked filets, we have computed the average shrinking coefficients for the length, width and height. These coefficients are: $L_{\text{cooked}}/L_{\text{raw}} = 0.86 \pm 0.02$, $H_{\text{cooked}}/H_{\text{raw}} = 0.93 \pm 0.02$, and $H_{\text{cooked}}/H_{\text{raw}} = 1.06 \pm 0.02$.

We observe that the chicken meat has shrunk substantially along the length — which is the main muscle fiber direction in chicken breast filet. Also there was shrinkage of the width, while the height of the meat has expanded due to the cooking. Such behavior has also been observed for beef (Goñi & Salvadori, 2010; Locker & Daines, 1976). It is attributed to the topology of the connective tissue (Locker & Daines, 1976). In a way the mechanical behavior of cooked meat is similar to materials with negative Poisson's ratio (Baughman, Stafström, Cui, & Dantas, 1998). Henceforth, it will be challenging to model this shrinkage behavior correctly using theories of mechanical deformation.

4.3. Cooking experiments

The recordings of the core and skin temperatures are shown in Figs. 8–10, where they are compared with the model predictions. The measurements on the mass of the chicken meat after the cooking experiment are listed in Table 2, also together with the model predictions, and the relative error in the model predictions. The presented experimental data is relative to the mass of the meat, prior to the cooking experiment. The mass losses are due to the cooking losses of water and evaporation.

From the experiments presented in Fig. 8 we observe that the core and surface temperatures reach a steady value after 20 min. This steady value is equal to the so-called wet bulb temperature, which is quite near the dew point of the air flowing over the chicken. Similar behaviors are shown in Figs. 9 and 10. Only the time to reach this steady state value depends on the airflow velocity, which determines the external heat transfer coefficient and thus the time scale of the energy transport. At extensive long cooking times one can observe that the surface temperature starts deviating from the wet bulb

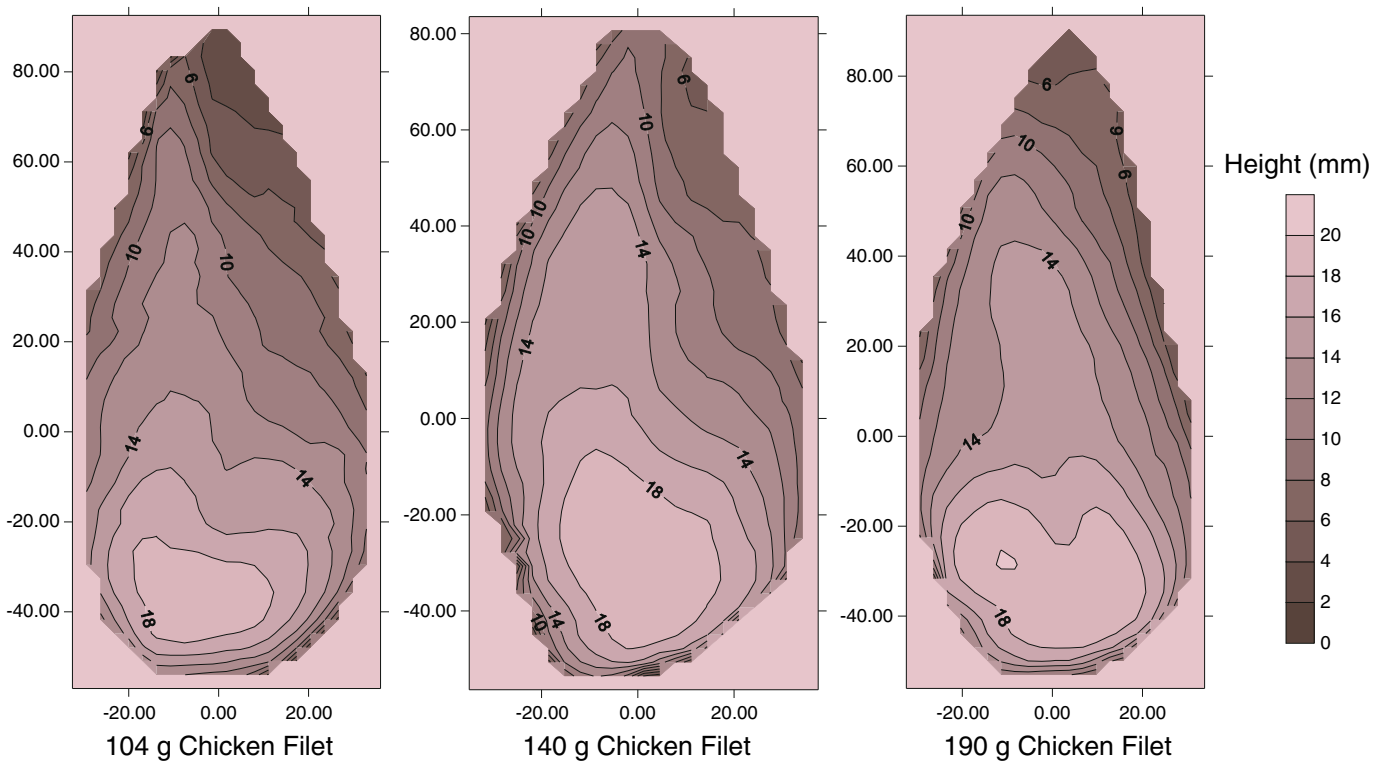

Fig. 6. Rescaled height maps of chicken filet of different masses. All dimensions are in [mm].

temperature because the water activity at the surface drops below unity. In that case, local equilibrium at the surface demands that the surface temperature rises. The surface temperature will approach the air temperature. After a lag time, the core temperature also starts rising. At air temperatures below boiling point the core temperature will also go towards the air temperature. At air temperatures above boiling point, internal evaporation occurs and the core temperature will remain at the boiling point, as shown in Fig. 10.

In drying one can observe also two regimes in the temperature behavior (Vagenas et al., 1990; Waananen et al., 1993). In the first regime, called the constant drying rate regime, the water activity is near unity and due to the evaporative cooling effect the surface temperature is at the wet bulb temperature. The water activity remains about unity for quite a large range of moisture content, as one can observe from the sorption isotherm in Fig. 14. After a while the moisture content comes in the range where the water activity drops sharply below unity. It has entered the falling drying rate regime. The surface temperature will rise gradually to the oven temperature. An evaporation front moves into the meat. At the evaporation front the temperature is at boiling point. From the center the temperature will rise to the boiling point.

A snapshot of the 3D simulation is shown in Fig. 11. The model is simulating here the experiment with an oven air temperature of $T_{\text{oven}} = 170$ °C, and dew point $T_{\text{dew}} = 90$ °C. The snapshot is taken

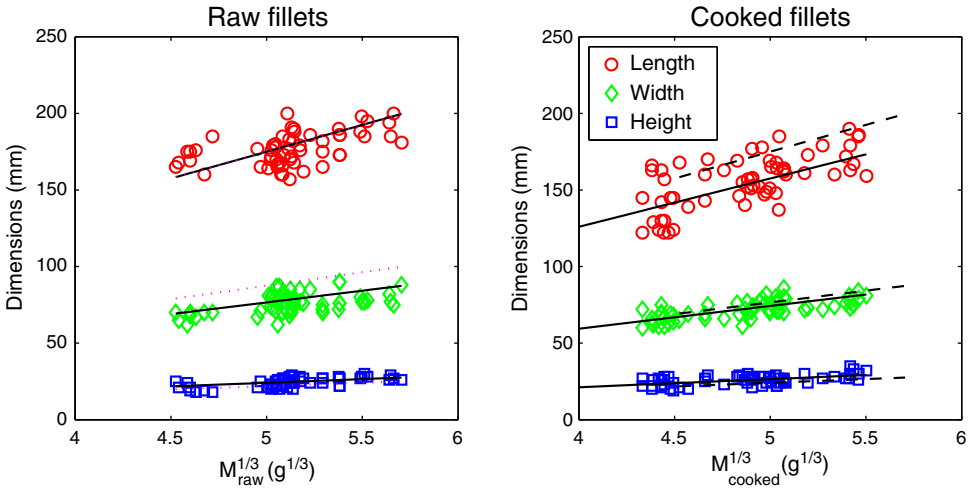

Fig. 7. Dimensions of chicken before and after experiment, as function of their mass. Symbols are the measured dimensions, and the solid lines are the fitted allometric scaling. The dotted lines in the left pane represent the scaling rules for the scanned filets, while the dashed lines in the right pane represent the fitted scaling rules for raw meat. Via comparison of the latter with the solid lines in the right pane, one can observe whether that dimension has undergone shrinkage.

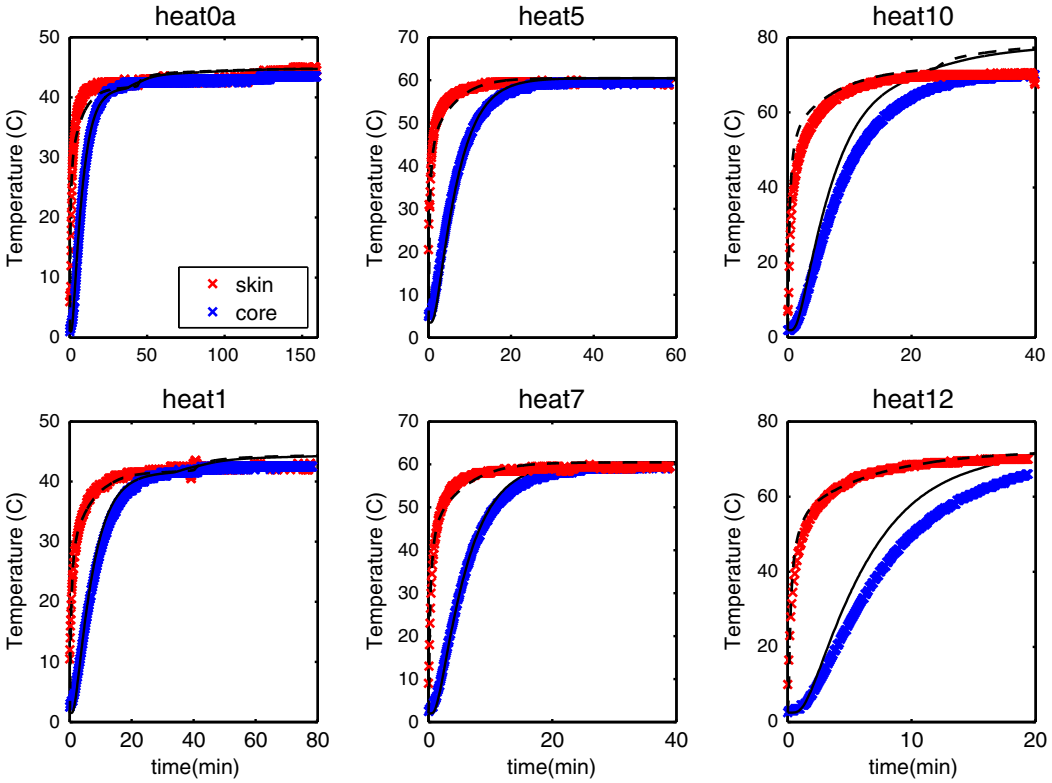

Fig. 8. Comparison of experimental (symbols) and numerical (lines) values of core and skin temperatures for experiments heat0a to heat12.

after 28 min of heating. Observe that the surface temperature is near boiling point, and drying out. We also want to notice the steep gradient in the moisture content.

The model predictions, presented in Figs. 8–10, are obtained after fitting the model to the experimental data via least squares. The parameter estimation is done via trial and error, as non-linear parameter

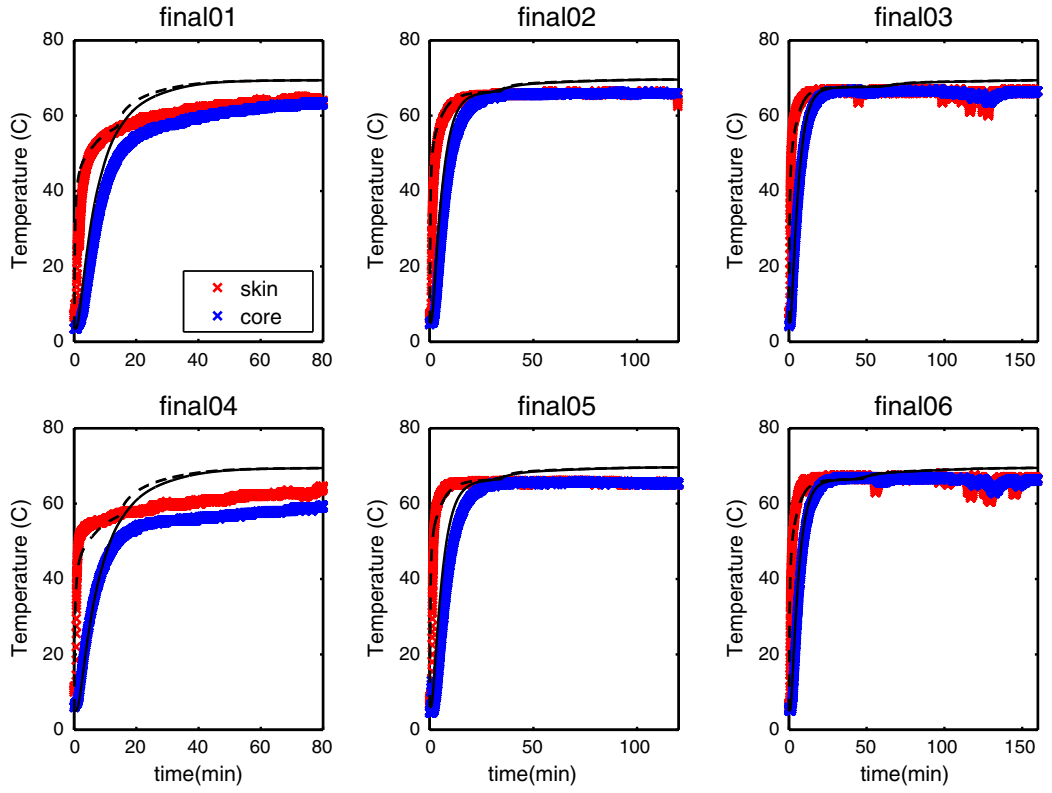

Fig. 9. Comparison of experimental (symbols) and numerical (lines) values of core and skin temperatures for experiments final01 to final06.

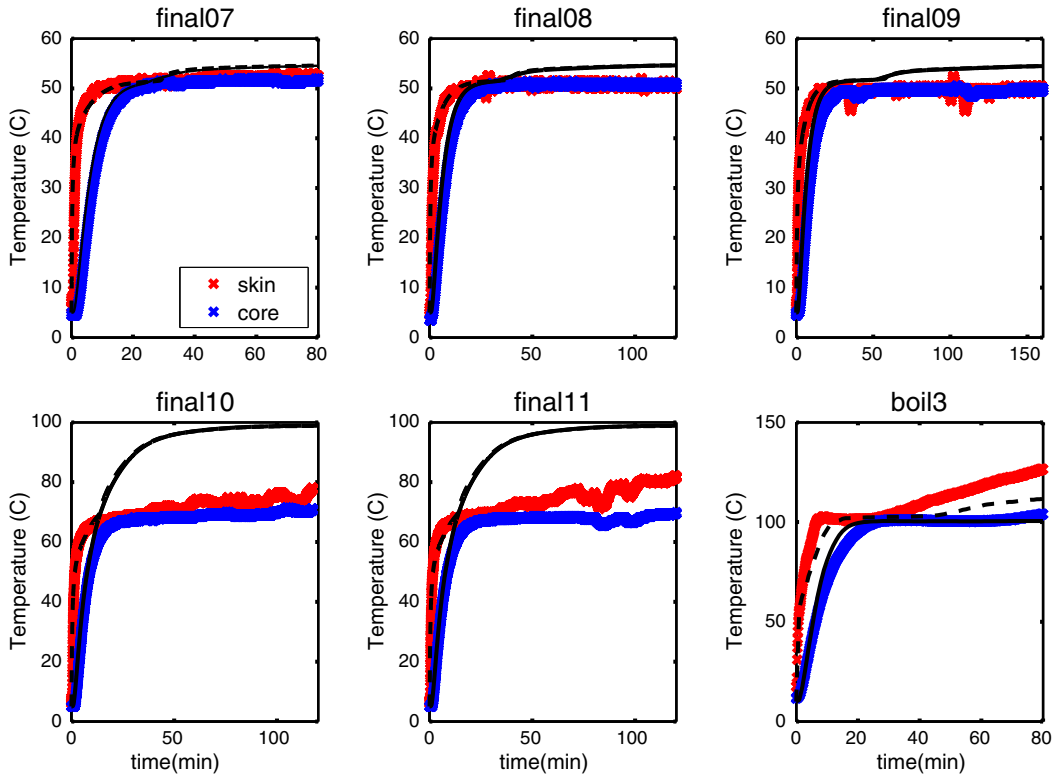

Fig. 10. Comparison of experimental (symbols) and numerical (lines) values of core and skin temperatures for experiments final07 to boil3.

estimation using Levenberg–Marquardt did not converge. Via manual minimization of the sum of squares we have obtained the following set of parameters:

$$a = 0.095 \pm 0.012;\ \ b = 4.0 \pm 1.1;\ \ \beta_1 = 0.040 \pm 0.005\ \ [\mathrm{m/s}] \qquad (29)$$

$$\frac{\kappa_0}{\nu} = 4.0 \pm 0.5 \times 10^{-6}\ \left[s^{-1}\right];\ \ D_{v,\mathrm{eff}} = 2.0 \pm 0.3 \times 10^{-7}\left[\mathrm{m^2/s}\right]. \qquad (30)$$

The errors in the estimated parameters are obtained via the Jacobian.

We recall that the first line of parameters are related to the heat and mass transfer coefficients, and the second line is related to the liquid and vapor transport in the pore space. Our analysis has shown that the heat transfer coefficient is *independent* of the airflow direction. Hence, in our model we have taken only the absolute value of the velocity in the correlation for the heat transfer coefficient. We note, that one can only identify the ratio κ_0/ν from the experiments, as we have no independent data on the viscosity of the expelled fluid (which contains possibly proteins, but which can also coagulate at higher temperatures).

From the comparison of the model predictions and experimental results in Figs. 8, 9 and 10, we conclude that the evolution of temperature is well predicted in the majority of the experiments, which are characterized by cooking times shorter or equal to 40 min. For these experiments also the prediction of the mass of the cooked meat is reasonably good. These values are within 5% of the experimental data, as shown in Table 2.

However, for some experiments there is a poor quantitative agreement between the model and the experiment. For the temperature the predictions start to deviate for times larger than 40 min, which is about the end of the constant drying rate regime. This group of experiments is characterized by:

- a long cooking time ($t_e \geq 80$ min),
- a large difference between oven temperature and dew point ($T_{\mathrm{oven}} - T_{\mathrm{dew}} \geq 20$ °C), and
- an excessive moisture loss.

For these experiments the model also fails to predict the mass of the cooked meat accurately. In Table 2 this group of experiments is indicated with asterisks. It appears that after reaching the falling drying rate regime, the model predicts too slow moisture transport. There is too little evaporative cooling effect, and the core temperature rises too quickly to the oven temperature. However, we do notice that the model predictions are *qualitatively* in agreement with the temperature behavior shown in the experiments. In the constant drying rate regime the surface temperature is at the wet bulb/dew point, and in the falling rate regime it gradually rises towards the oven temperature. Such behavior is

Table 2
Setup of the cooking experiments.

Index	M_{exp}% (g/g)	M_{model}% (g/g)	Prediction error (%)
heat0a	87	88	1.1
heat1	94	90	4.2
heat5	96	99	3.1
heat7	96	99	3.1
heat10[a]	89	89	0.0
heat12	94	92	2.1
final01[a]	75	85	13.3
final02	88	88	0.0
final03	84	88	4.8
final04[a]	78	86	10.2
final05	85	87	2.4
final06	80	86	7.5
final07	87	89	2.3
final08[a]	96	91	5.2
final09[a]	95	88	7.4
final10[a]	64	78	22
final11[a]	65	79	22
boil3	38	57	50

[a] Experiments where model does not give a good prediction of temperature.

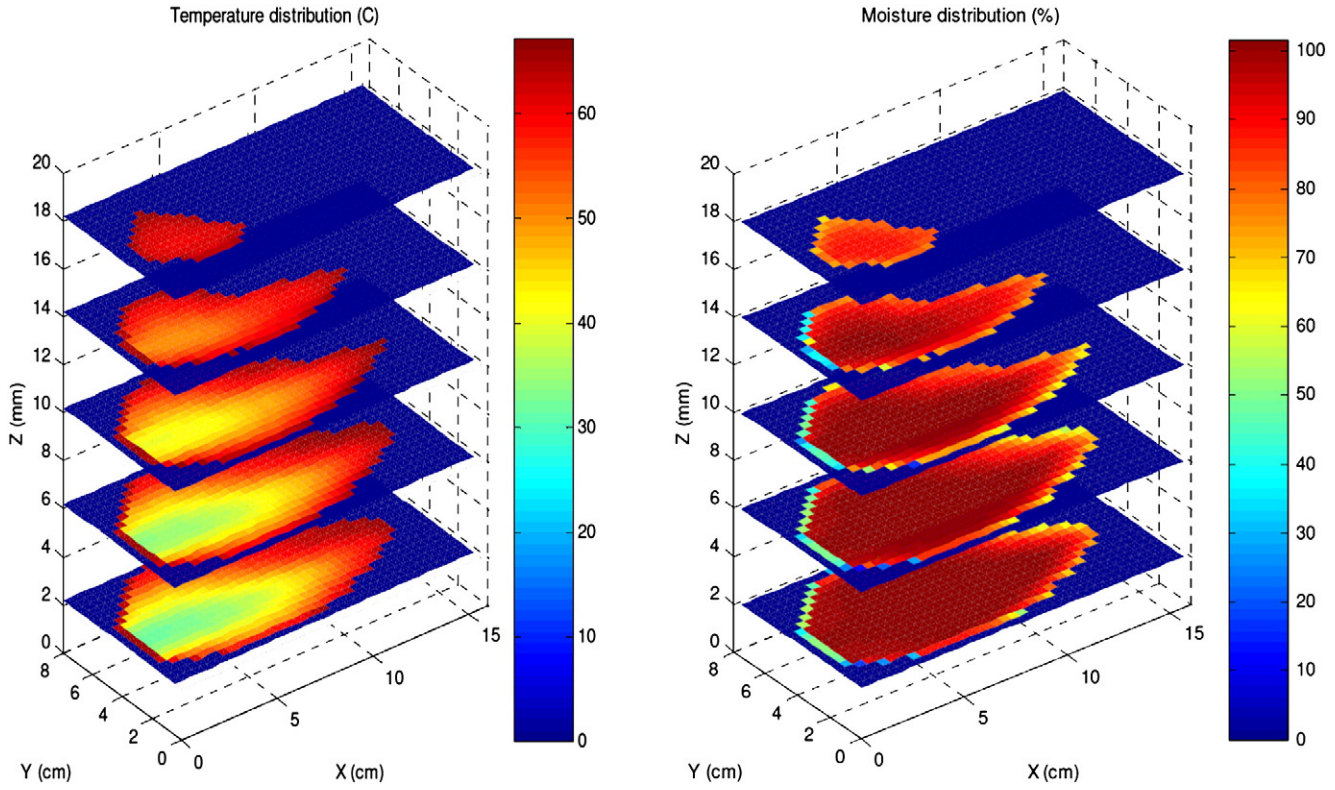

Fig. 11. Visualization of simulation results, showing the temperature T and water mass fraction (y_w) distribution in various horizontal cross sections. Experiments are performed at $T_{oven} = 170$ °C and $T_{dew} = 90$ °C. The snapshot is taken after 28 min of heating.

especially clear in the last pane of Fig. 10, where the oven temperature is above boiling point, as well as in earlier studies (Murphy et al., 2001).

5. Discussion

5.1. Model predictions of meat cooking

Similar to the previous studies using the water demand model (Feyissa et al., 2013; Goñi & Salvadori, 2010; van der Sman, 2007a), we have shown in this paper, that the model based on the swelling pressure gradients can accurately predict the temperature evolution and moisture loss during meat cooking at oven temperatures below boiling point and at industrial relevant cooking times. In cases of meat cooking at oven temperatures above boiling points or long cooking times capillary transport becomes important. The model captures the enhanced physics of the meat cooking problem only in a qualitative way. We expect that the current model misses some essential element in the dynamics of the moisture transport.

Recent experimental investigations of moisture transport during meat cooking are hinting at the missing link: the temporal evolution of the permeability (Bouhrara et al., 2011; Feyissa et al., 2013). At temperatures above 40°, when myosin starts denaturing, MRI shows the formation of drip channels. When myosin denatures the myofibers shrink, and the excess liquid is expelled from the intracellular space into the extracellular space. At a further increase of temperature, the width of the drip channels is increased (Bouhrara et al., 2011). Microscopic images of the texture of cooked meat from Feyissa et al. (2013) strongly resemble the crack pattern induced by fracturing phase separation in soft matter (Tanaka, 2012). At temperatures above 55° the collagen of the endomysium connective tissue starts to contract and solubilize (Bouhrara, Clerjon, Damez, Kondjoyan, & Bonny, 2012), which weakens the connections between the layers of the connective tissue (endomysium and perimysium) (Lewis & Purslow, 1990). The shrinking myofiber lattice imparts stress on these connections, which fractures and enlarges the extracellular space.

Capillary transport happens in the extracellular space. Hence, the increase of the drip channels has important consequences for the capillary moisture transport, as the increased width leads to a higher permeability κ_0. Our model is clearly missing this aspect. Furthermore, the assumption that the amount of capillary water is negligible is not valid anymore, when significant drip channels are formed. If the capillary transport is more enhanced than assumed in our model, there can be sufficient moisture transport from the core to the surface to keep the core temperature longer at the wet bulb temperature via evaporative cooling at the internal evaporation front, as is shown in our experiments. The enhanced capillary transport can also explain the enhanced moisture loss observed in the experiments, as shown in Table 1.

Another essential, missing element in our current model is a description of the shrinkage of the meat. Our experimental data on the change of the dimensions of the chicken meat upon cooking shows that the modeling of shrinkage will be very challenging. Meat is not shrinking isotropically, and is even expanding in the height — while shrinking in its length and width. Similar to materials with negative Poisson's ratio the cause of this anisotropy in shrinkage must be found in the microstructure of the material. The hierarchical structure of the connective tissue has some resemblance of the microstructure of such materials (Rowe, 1981). Hence, the aspects of the microstructure of the meat have to be taken into account in the modeling.

5.2. Outlook on prediction of WHC

Recent works (Kristinsson & Hultin, 2003; Puolanne & Halonen, 2010) show that there are four major hypotheses, which are said to determine the WHC of meat products: 1) electrostatic repulsion between protein fibers (Hamm & Deatherage, 1960), 2) osmotic pull of water (Offer et al., 1989), 3) restraining mechanical (elastic) forces

of the protein matrix and 4) water held in pores by capillary forces (Hermansson & Lucisano, 1982; Offer & Trinick, 1983; Tornberg, 2005). However, there is no commonly accepted theory explaining the WHC of meat products, or protein gels in general. Some researchers attribute the WHC totally to capillary forces, while it is strongly questioned by others (Stevenson, Dykstra, & Lanier, 2013, Stevenson, Liu, & Lanier, 2012).

We argue that all four mechanisms contribute to the WHC. The first three contributions can be described by the Flory–Rehner theory. The fourth contribution is described by the Young–Laplace law. In equilibrium the swelling pressure from the Flory–Rehner theory is equal to the capillary pressure as follows from the Young–Laplace law. From the discussion of the model prediction follows that the amount of capillary water in drip channels is much more significant than we have assumed previously, and thus could give a significant contribution to the WHC. Like protein gels, meat must be considered as a two-phase (microphase-separated) system (Leksrisompong et al., 2012).

In this and earlier papers (van der Sman, 2007a, 2007b) we have considered meat, which is at natural post-mortem pH levels (about 5.8, near the isoelectric point) with no salts added. Flory–Rehner theory can be extended to cope with different pH levels and ionic strengths (Mercadé-Prieto, Falconer, Paterson, & Wilson, 2007), recognizing the polyelectrolyte nature of meat proteins. In the above theory, we have also assumed that the effect of electrostatic forces between proteins can be absorbed into an effective Flory–Huggins interaction parameter. This approximation is okay at moderate to high concentrations of salts (Mercadé-Prieto et al., 2007). In our recent study we have also investigated high-salt meat products, where the osmotic effects of the dissolved salts exceed the contribution of the electrostatic repulsion between protein fibers (due to the electrostatic screening effects) (van der Sman, 2012a).

In the extended Flory–Rehner theory the ionic contribution to the swelling pressure is described by:

$$\Pi_{\text{ion}} = \nu_w RT \frac{a_0^2 \phi^2}{a_0 \phi + 4I} \tag{31}$$

with I the ionic strength of the solution. In the high-salt limit it is linear with ϕ^2, while in the low-salt limit it is linear with the fixed charge of the polyelectrolyte. a_0 is a measure of the surface charge, which depends on pH — and is linear with the degree of ionization $i_{\pm}$. There is a condition for chemical equilibrium:

$$i_{\pm} = \frac{1}{1 + K_p 10^{\text{pH}-14}}. \tag{32}$$

The constant K_p depends on the isoelectric point of the protein (pI).

A comprehensive discussion of biomaterials like meat as polyelectrolyte gels is given by Elliott and Hodson (1999). They discuss them also from the viewpoint of Flory–Rehner theory. Furthermore, they discuss counterion condensation, and specific transient anion binding (chloride or phosphate) — which changes the surface charge of proteins. This explains why NaCl shifts the pI of meat (Puolanne & Peltonen, 2013).

Viewing protein correctly as a polyelectrolyte gel will explain the observations on the change of water holding capacity via marination (i.e., addition of salts and acidification) (Barbanti & Pasquini, 2005; Gault, 1985; Schmidt, Carciofi, & Laurindo, 2008). A few studies are about changes in water holding capacity considering that meat has gel-like properties, which can be tuned. The Flory–Rehner theory states that WHC can be changed via altering the number of crosslinks. This can be done via proteolytic enzymes (Farouk, Mustafa, Wu, & Krsinic, 2012; Naveena, Mendiratta, & Anjaneyulu, 2004), or via crosslinking enzymes (Chanarat, Benjakul, & Kittikun, 2012). Proteolytic enzymes as from plant sources like papaya, or endogenous to meat (calpains) hydrolyze the crosslinking protein structures, and decrease the number of crosslinks — which increases the water holding capacity. Hence, the Flory–Rehner theory also explains the "sponge effect" occurring during aging of meat (Farouk et al., 2012) Crosslinking enzymes like transglutaminase or tyrosinase increase the number of crosslinks, and decrease the WHC — while making the texture more firm (Chanarat et al., 2012; Lantto, Puolanne, Kruus, Buchert, & Autio, 2007).

In our calculations, we have implicitly assumed that protein denaturation is instantaneous and irreversible. Recent studies show that one might question these assumptions. A first indication is given by the fact that the time evolution of cooking loss or juiciness is much longer than the time required for the meat temperature to equilibrate with the environment (Mortensen, Frøst, Skibsted, & Risbo, 2012; Oillic, Lemoine, Gros, & Kondjoyan, 2011; Skipnes, Johnsen, Skåra, Sivertsvik and Lekang, 2011). It might be that this is due to a longer time scale for moisture transport through the capillaries. However, the samples studied by Mortensen et al. (2012) have a thickness of only 2 cm. The time scale of moisture transport is not expected to be in the order of 12 h for moderate temperature of 56–60°. We argue that the long time scale of the evolution of cooking loss is due to the dynamics in the protein denaturation. In recent kinetic models of meat protein denaturation, the time scale of denaturation (the inverse of the reaction rate) is in the order of 15–30 min at 60° (de Moraes & Cunha, 2013; Dima, Barón, & Zaritzky, 2012; Skipnes, Van der Plancken, Van Loey, & Hendrickx, 2008). Hence, the denaturation of meat proteins is not instantaneous, and might even be partially reversible (de Moraes & Cunha, 2013). Hence, next to temperature, the cooking time is an important process condition to control the WHC. This is particularly used in the long-time-low-temperature treatments of meat during sous-vide cooking, as practiced by chef–cooks following the trend of molecular gastronomy (Mortensen et al., 2012). The kinetics of protein denaturation might well be coupled to the presented model based on the Flory–Rehner theory. The protein denaturation kinetics must be linked to the change of the Flory–Huggins interaction parameter, which is a measure of the (surface) hydrophobicity of the protein, and thus the state of its denaturation.

6. Conclusions

Similar to other recent studies (Feyissa et al., 2013; Goñi & Salvadori, 2010; van der Sman, 2007a), we have shown that the model of meat cooking based on the swelling pressure as calculated from the Flory–Rehner theory (or its approximation using the "water demand") can well explain the temperature evolution and moisture loss for cooking temperatures below boiling point and practical relevant cooking times (less than 1 h).

The discrepancy between model and experiments at high cooking temperatures (above boiling point) or very long cooking times indicate that our current model underestimates the amount of capillary water and its transport rate. Recent studies show that during heating drip channels develop, whose width increase with temperature (Bouhrara et al., 2011). Future models must account for the dynamics in the permeability of the drip channels.

The dynamics of the geometry of the drip channels is intimately linked to the mechanical deformation of meat, induced by the shrinking proteins. Our observations of the macroscopic deformation of the cooked chicken filet shows very intricate mechanical behavior of meat: while shrinking in length and width, it increases in height. Meat bears quite some resemblance to negative Poisson's ratio materials. It is likely that truly predictive models must account for the process on both the macroscopic (product) scale, and the mesoscopic (pore) scale — utilizing a multiscale simulation framework (Buehler, 2010; Buehler & Ackbarow, 2007; Datta et al., 2012; Ho et al., 2013).

The validity of the Flory–Rehner theory for explaining the WHC of non-marinated meat is shown in our recent paper (van der Sman, 2012a). In our extensive discussion we have shown that the Flory–Rehner theory provides the physical basis for explaining how the changes of the WHC by pH, salts, enzymes, and kinetics in protein denaturation are brought about. The ingredients which can alter the WHC are conveniently introduced into the meat via impregnation techniques (Chiralt et al., 2001; Schmidt, Carciofi, & Laurindo, 2009). As this is also a pressure driven process, one can describe that with a model similar to the one presented in this paper.

Appendix A. Constitutive relations

A.1. Water holding capacity

From the water holding capacity data, we have computed the volume fraction of the polymer ϕ_p. These data, together with other data on water holding capacity of other mammalian meat, we have fitted to the Flory–Rehner theory (van der Sman, 2012b). All these different kinds of meat behave quite similarly. From the data we have determined the temperature dependency of the Flory–Huggins interaction parameter and the parameters related to the elastic contribution to the swelling pressure.

For the change of the interaction parameter with temperature, we have assumed that it follows a similar dependency as for the water holding capacity, which we have taken from our earlier paper (van der Sman, 2007a):

$$\chi_{p,1}(T) = \chi^N_{p,1} + \frac{\chi^D_{p,1} - \chi^N_{p,1}}{1 + 30\exp(-0.25(T - T_e))} \tag{33}$$

with $T_e = 325K$. $\chi^N_{p,1}$ is the interaction parameter for the dry, *native* protein, which is $\chi^N_{p,1} = 0.8$ – similar to polysaccharides (van der Sman & Meinders, 2011). $\chi^D_{p,1} = 1.4$ is the interaction parameter for the *protected denatured* proteins. It appears that the denatured proteins have a universal value of 1.4 for their interaction parameter (van der Sman et al., submitted for publication).

The values of the other model parameters are: $\phi_0 = 0.6$ and $E_0 = 20$ MPa. In Fig. 12 we show a) the prediction of Flory–Rehner theory of the WHC compared to the experimental data from various kinds of meat, and b) the temperature dependency of χ_p.

A.2. Glass transition

For the prediction of the free volume contribution to the water activity, we require the glass transition temperature as a function of moisture content. The glass transition of meat, being a mixture of water and hydrophilic proteins, has been described by the Couchman–Karasz relation (van der Sman, 2012b):

$$T_g = \frac{y_w \Delta C_{p,w} T_{g,w} + y_s \Delta C_{p,s} T_{g,s}}{y_w \Delta C_{p,w} + y_s \Delta C_{p,s}} \tag{34}$$

$\Delta C_{p,w} = 1.94$ kJ/kg · K, $\Delta C_{p,s} = 0.42$ kJ/kg · K, $T_{g,w} = 139$ K, and $T_{g,s} = 475$ K. The data on the glass transition are shown in Fig. 13, which has been reproduced from van der Sman (2012b).

A.3. Water activity

The water activity of raw and pre-cooked meat at room temperature is shown in Fig. 14, which has also been reproduced from van der Sman (2012b). It has been modeled with the Flory–Huggins-free-volume theory with a temperature dependent interaction parameter for the proteins.

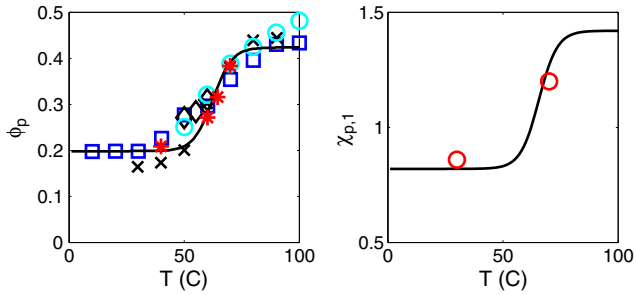

Fig. 12. a) Water holding capacity, as expressed in protein volume fraction $\phi_p = 1 - \phi_w$, as function of temperature, and b) Flory–Huggins interaction parameter $\chi_{p,1}$ as function of temperature. Our experimental data on the WHC of chicken meat are indicated with the red symbols (asterisks).
The figure is adapted from Ref. van der Sman (2012a).

A.4. Capillary pressure

We derive the constitutive relation for the capillary pressure using the assumption that the structure of meat can be approximated as an array of cylinders with hexagonal packing – which is fully wetted by water. The geometry of the pore space fully determines the relation between capillary pressure and the saturation, and follows from Lago and Araujo (2003). The radius of the fiber is denoted as R. The unit cell of the hexagonal packing is an equilateral triangle of sides $2R$. The total cross sectional area is $A = \sqrt{3}R^2$. The area for the pore space is $A_p = A - \pi R^2/2 \approx 0.16R^2$. Hence, the total capillary water is negligible compared to the absorbed water, as $A_p \ll A$. The fraction S_w of the pore space is filled with liquid. The contact line of the liquid–gas interface makes an angle of $\frac{1}{2}\beta$, with the line connecting the centers of the fibers. In Fig. 15, we have depicted the unit cell and the defined angles and dimensions.

The curvature r of liquid–gas interface is a function of angle β:

$$\frac{r}{R} = \frac{1 - \cos(\beta)}{\cos(\beta)} \tag{35}$$

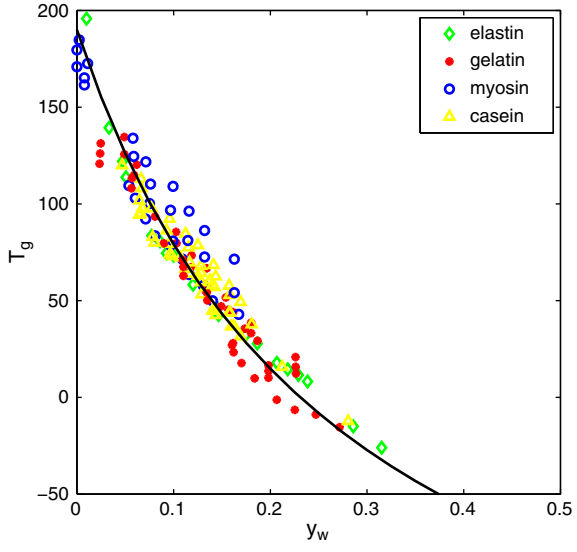

Fig. 13. Glass transition temperature T_g as a function of mass fraction of water y_w for various proteins of animal origin. All data can be fitted with a single curve, which follows the Couchman–Karasz theory.

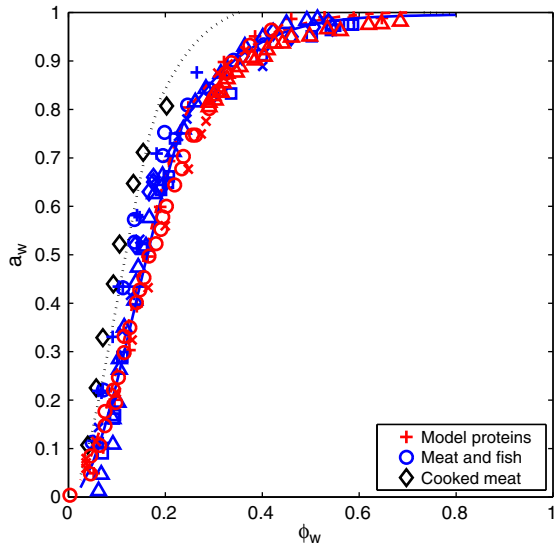

Fig. 14. Sorption isotherms of different proteins. Red curve and symbols are for model proteins ($\chi_1 = 0.76$), and blue curve and symbols are for lean meat products ($\chi_1 = 0.86$). The dashed curve is the sorption isotherm for precooked meat, which is fitted with $\chi_1 = 1.2$.

with $0 < \beta < \pi/6$, and consequently $r_{max}/R \leq 0.155$. At this stage the saturation is:

$$S_{w,max} = \frac{A_p - \pi r_{max}^2}{A_p} = 1 - \pi 0.155 \approx 0.5. \tag{36}$$

The wetted area as function of β:

$$A_w = R^2\left[\sin(2\beta) - 2\beta + 4\cos(\beta)\sin(\beta)r/R + (\sin(2\beta) - 2\beta + \pi)(r/R)^2\right]. \tag{37}$$

We have plotted this relation and compared that with the empirical van Genuchten relation (Parker, Lenhard, & Kuppusamy, 1987), which states:

$$\frac{p_{cap}R}{\sigma} = B\left(S_{w,eff}^{n} - 1\right)^{m}. \tag{38}$$

This relation goes to the expected limit of $p_{cap} = 0$ for $S_w = 1$. This is because at the evaporation front the curvature of the water/gas interphase is flat. This limit does not hold for the relation of Araujo and Lago. Hence, we take the van Genuchten relation, and fitted that closely to the model of Araujo and Lago. Using regression we have obtained $B = 6$, $n = -1.29$, and $m = 0.5$. In reality deviations from the theoretical curve of Araujo and Lago are expected, due to variation in the dimensions amongst the various pores.

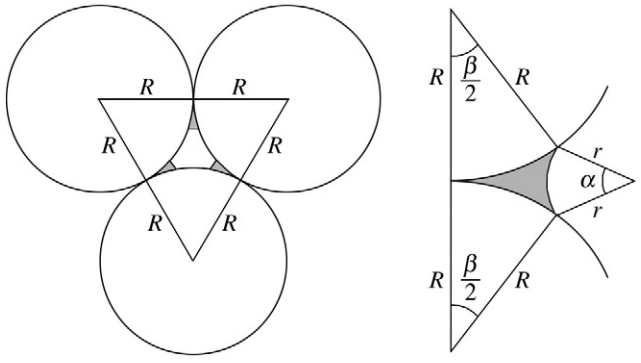

Fig. 15. Geometry of the pore space, the interspaces in a hexagonal array of cylinders of radius R, containing the capillary water with curvature r.

A.5. Relative permeability

If a gas phase is present ($S_w < 1$) the permeability of the pore space becomes lower. The relative permeability as a function of water saturation is given by Ni et al. (1999):

$$\kappa_w = \left(\frac{S_w - S_{irr}}{1 - S_{irr}}\right)^3 \kappa_{w,0} \tag{39}$$

where S_{irr} is the so-called irreducible water saturation, which is normally $S_{irr} = 0.09$ for food products (Ni et al., 1999). Often one defines $S_{w,eff} = (S_w - S_{irr})(1 - S_{irr})$. For $S_w < S_{irr}$ $k_{w,r} = 0$, and $k_{v,r} = 1$.The relative vapor permeability as function of water saturation is given by:

$$k_{v,r} = 1 - \frac{S_w}{1 - S_{irr}}. \tag{40}$$

A.6. Thermal conductivity

The thermophysical properties of (roasting) meat can be fully characterized by its composition, and knowledge about the direction of the meat fibers (Choi & Okos, 1986; van der Sman, 2008; van der Sman & Boer, 2005). We assume that the fibers are all oriented along the length axis of the meat (Fig. 16). For the heat conductivity along the fibers $\lambda_{||}$, we assume the parallel model:

$$\lambda_{||} = \left(1 - \epsilon\right)\lambda_s + S_w\epsilon\lambda_w + (1 - S_w)\epsilon\lambda_g \tag{41}$$

and for the heat conductivity perpendicular to the fibers, $\lambda_{\perp}$, we assume the serial model:

$$\frac{1}{\lambda_{\perp}} = \frac{(1-\epsilon)}{\lambda_s} + \frac{S_w\epsilon}{\lambda_w} + \frac{(1 - S_w)\epsilon}{\lambda_g} \tag{42}$$

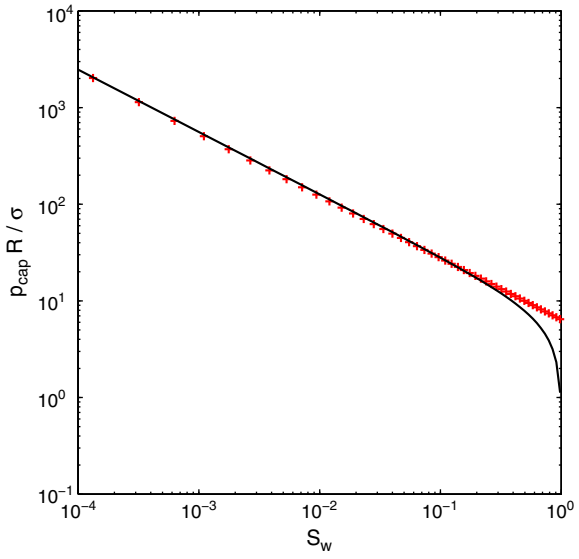

Fig. 16. The capillary pressure p_{cap} versus water saturation S_w in meat, according to 1) the relation of Lago and Araujo for hexagonal array of cylinders (symbols), and 2) its approximation with the van Genuchten relation (solid line).

with the porosity of the meat, λ_s the effective thermal conductivity of the solid phase (consisting of proteins and absorbed water), and λ_g the thermal conductivity of the gas (consisting of water vapor and air). Because we have neglected the shrinkage of the meat, the porosity is assumed to be constant in the model. The saturation S_w will be determined by the local thermodynamic equilibrium.

For the thermal conductivity of the solid phase λ_s, we assume the perfect mixture model:

$$\frac{1}{\lambda_s} = \frac{1-\phi_p}{\lambda_w} + \frac{\phi_p}{\lambda_p}. \tag{43}$$

Here λ_w is the conductivity of water and λ_p is the conductivity of proteins. ϕ_b is the volume fraction of the proteins, which is computed as:

$$\phi_b = \frac{y_b/\rho_w}{y_b/\rho_w + y_p/\rho_p} \tag{44}$$

with y_b the mass fraction of absorbed water, and y_p the mass fraction of the protein in the solid phase.

For the gas phase we also assume a perfect mixture model. The gas may consist of air and vapor. It is characterized by the total gas pressure p_{gas} and the water vapor pressure p_v. Defining the volume fraction $\phi_v = p_v/p_{\text{gas}}$ the conductivity of the gas is:

$$\frac{1}{\lambda_g} = \frac{\phi_v}{\lambda_v} + \frac{1-\phi_v}{\lambda_a}. \tag{45}$$

Here λ_v is the conductivity of water vapor and λ_a is the conductivity of air, which are known functions of temperature (Choi & Okos, 1986; van der Sman, 2008; van der Sman & Boer, 2005).

In Fig. 17 we have plotted the thermal conductivity as a function of moisture content, at a boiling point of water (100 °C). We have observed the sharp decrease in conductivity perpendicular to the fibers.

A.7. Heat and mass transfer coefficients

As usual in engineering science the transfer coefficients will be determined from a correlation between Nusselt number *Nu* (or Sherwood number *Sh*) and Reynolds number *Re* and Prandtl number *Pr*. We take the correlations for turbulent flow over a flat surface (Bird, Stewart, & Lightfoot, 2006), but with the prefactor *a* as a fitting parameter to account for the finite size of the chicken meat:

$$\begin{aligned} Nu &= aRe^{0.8}Pr^{0.33} \\ Sh &= aRe^{0.8}Sc^{0.33}. \end{aligned} \tag{46}$$

For (hot) air holds that $Pr^{0.33}, Sc^{0.33} \approx 1$. As length scale for the Reynolds and Nusselt numbers is taken the length of the filet L:

$$\begin{aligned} Re &= \frac{v_{\text{air}}L}{\nu_{\text{air}}} \\ Nu &= \frac{\alpha_{\text{ext}}L}{\lambda_{\text{air}}} \\ Sh &= \frac{\beta_{\text{ext}}L}{D_v}. \end{aligned} \tag{47}$$

We also assume that β_{skin} is dependent on the local moisture content of the meat y_w, and will show a large decrease if it goes through a glass transition. During experiments at oven temperatures $T_{\text{oven}} < 40$ °C, it has been observed that the skin of the filet indeed becomes glassy. We have used the following empirical correlation (not based on physical principles)

$$\beta_{\text{skin}} = \beta_1 y_w^b. \tag{48}$$

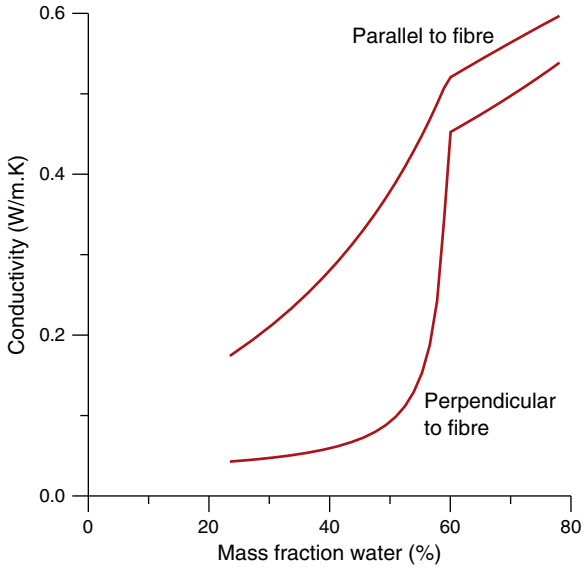

Fig. 17. Thermal conductivity of chicken meat as a function of mass fraction of water at $T = 100$ °C, perpendicular and parallel to the meat fibers. Values are computed according to the model as described in Appendix A.

The exponent *b* will be determined via fitting the model to the experimental data.

References

Aliño, M., Grau, R., Fernández-Sánchez, A., Arnold, A., & Barat, J. M. (2010). Influence of brine concentration on swelling pressure of pork meat throughout salting. *Meat Science*, *860*(3), 600–606.

Aregawi, Wondwosen Abebe, Defraeye, Thijs, Verboven, Pieter, Herremans, Els, De Roeck, Guido, & Nicolai, B. M. (2012). Modeling of coupled water transport and large deformation during dehydration of apple tissue. *Food and Bioprocess Technology*, 1–16.

Ball, Philip (2008). Water as an active constituent in cell biology. *Chemical Reviews*, *1080*(1), 74–108.

Barbanti, D., & Pasquini, M. (2005). Influence of cooking conditions on cooking loss and tenderness of raw and marinated chicken breast meat. *LWT — Food Science and Technology*, *380*(8), 895–901.

Baughman, R. H., Stafström, S., Cui, C., & Dantas, S. O. (1998). Materials with negative compressibilities in one or more dimensions. *Science*, *2790*(5356), 1522–1524.

Baulin, V. A., & Halperin, A. (2002). Concentration dependence of the flory ξ parameter within two-state models. *Macromolecules*, *350*(16), 6432–6438.

Bekiranov, Stefan, Bruinsma, Robijn, & Pincus, Philip (1997). Solution behavior of polyethylene oxide in water as a function of temperature and pressure. *Physical Review E*, *550*(1), 577.

Bird, R. B., Stewart, W. E., & Lightfoot, E. N. (2006). *Transport phenomena.* Wiley.

Block, William (2003). Water or ice — The challenge for invertebrate cold survival. *Science Progress*, *860*(1–2), 1–2.

Bouhrara, M., Clerjon, S., Damez, J. L., Chevarin, C., Portanguen, S., Kondjoyan, A., & Bonny, J. M. (2011). Dynamic MRI and thermal simulation to interpret deformation and water transfer in meat during heating. *Journal of Agricultural and Food Chemistry*, *590*(4), 1229–1235.

Bouhrara, M., Clerjon, S., Damez, J. L., Kondjoyan, A., & Bonny, J. M. (2012). In situ imaging highlights local structural changes during heating: The case of meat. *Journal of Agricultural and Food Chemistry*, *600*(18), 4678–4687.

Buehler, M. J. (2010). Multiscale mechanics of biological and biologically inspired materials and structures. *Acta Mechanica Solida Sinica*, *230*(6), 471–483.

Buehler, M. J., & Ackbarow, T. (2007). Fracture mechanics of protein materials. *Materials Today*, *100*(9), 46–58.

Chanarat, S., Benjakul, S., & Kittikun, A. H. (2012). Comparative study on protein cross-linking and gel enhancing effect of microbial transglutaminase on surimi from different fish. *Journal of the Science of Food and Agriculture*, *920*(4), 844–852.

Chiralt, A., Fito, P., Barat, J. M., Andres, A., González-Martınez, C., Escriche, I., & Camacho, M. M. (2001). Use of vacuum impregnation in food salting process. *Journal of Food Engineering*, *490*(2), 141–151.

Choi, Y., & Okos, M. R. (1986). Effects of temperature and composition on the thermal properties of foods. *Food Engineering and Process Applications*, *1*, 93–101.

Chou, David H., & Morr, Charles V. (1979). Protein–water interactions and functional properties. *Journal of the American Oil Chemists' Society*, *560*(1), 53–62.

Datta, A. K. (2007). Porous media approaches to studying simultaneous heat and mass transfer in food processes. I: Problem formulations. *Journal of Food Engineering*, *800*(1), 80–95.

Datta, A. K., van der Sman, R., Gulati, T., & Warning, A. (2012). Soft matter approaches as enablers for food macroscale simulation. *Faraday Discussions*, *158*, 435.

De Gennes, P. G. (1991). A second type of phase separation in polymer solutions. *Comptes rendus de l'Académie des sciences. Série 2, Mécanique, Physique, Chimie, Sciences de l'univers, Sciences de la Terre*, *3130*(10), 1117–1122.
de Moraes, M. C., & Cunha, R. L. (2013). Gelation property and water holding capacity of heat-treated collagen at different temperature and pH values. *Food Research International*, *500*(1), 213–223.
Dhall, A., & Datta, A. K. (2011). Transport in deformable food materials: A poromechanics approach. *Chemical Engineering Science*, *660*(24), 6482–6497.
Dhall, A., Halder, A., & Datta, A. K. (2012). Multiphase and multicomponent transport with phase change during meat cooking. *Journal of Food Engineering*, *1130*(2), 299–309.
Dima, J. B., Barón, P. J., & Zaritzky, N. E. (2012). Mathematical modeling of the heat transfer process and protein denaturation during the thermal treatment of Patagonian marine crabs. *Journal of Food Engineering*, *1130*(4), 623–634.
Dinčov, D. D., Parrott, K. A., & Pericleous, K. A. (2004). Heat and mass transfer in two-phase porous materials under intensive microwave heating. *Journal of Food Engineering*, *650*(3), 403–412.
Elliott, G. F., & Hodson, S. A. (1999). Cornea, and the swelling of polyelectrolyte gels of biological interest. *Reports on Progress in Physics*, *610*(10), 1325.
Farkas, B. E., Singh, R. P., & Rumsey, T. R. (1996). Modeling heat and mass transfer in immersion frying. I, model development. *Journal of Food Engineering*, *290*(2), 211–226.
Farouk, M. M., Mustafa, N. M., Wu, G., & Krsinic, G. (2012). The "sponge effect" hypothesis: An alternative explanation of the improvement in the waterholding capacity of meat with ageing. *Meat Science*, *900*(3), 670.
Feyissa, A. H. (2011). *Robust modeling of heat and mass transfer in processing of solid foods.* : Technical University of Denmark, Department of Systems Biology.
Feyissa, A. H., Gernaey, K. V., & Adler-Nissen, J. (2013). 3D modeling of coupled mass and heat transfer of a convection-oven roasting process. *Meat Science*, *930*(4), 810–820.
Flory, P. J. (1942). Thermodynamics of high polymer solutions. *The Journal of Chemical Physics*, *10*, 51.
Flory, P. J., & Rehner, J., Jr. (1943). Statistical mechanics of cross-linked polymer networks II. Swelling. *The Journal of Chemical Physics*, *11*, 521.
Gault, N. F. S. (1985). The relationship between water-holding capacity and cooked meat tenderness in some beef muscles as influenced by acidic conditions below the ultimate pH. *Meat Science*, *150*(1), 15–30.
Goñi, S. M., & Salvadori, V. O. (2010). Prediction of cooking times and weight losses during meat roasting. *Journal of Food Engineering*, *1000*(1), 1–11.
Halle, Bertil (2004). Protein hydration dynamics in solution: A critical survey. *Philosophical Transactions of the Royal Society of London. Series B, Biological Sciences*, *3590*(1448), 1207–1224.
Hamm, R., & Deatherage, F. E. (1960). Changes in hydration, solubility and charges of muscle proteins during heating of meat. *Journal of Food Science*, *250*(5), 587–610.
He, X., Fowler, A., & Toner, M. (2006). Water activity and mobility in solutions of glycerol and small molecular weight sugars: Implication for cryo-and lyopreservation. *Journal of Applied Physics*, *1000*(7) 074702-074702.
Hermansson, A., & Lucisano, M. (1982). Gel characteristics–water binding properties of blood plasma gels and methodological aspects on the water binding of gel systems. *Journal of Food Science*, *470*(6), 1955–1959.
Hills, Brian P., Manning, Charles E., & Ridge, Yvonne (1996). New theory of water activity in heterogeneous systems. *Journal of the Chemical Society, Faraday Transactions*, *920*(6), 979–983.
Ho, Q. T., Carmeliet, J., Datta, A. K., Defraeye, T., Delele, M. A., Herremans, E., Opara, L., Ramon, H., Tijskens, E., van der Sman, R., van Liedekerke, P., Verboven, P., & Nicolai, B. M. (2013). Multiscale modeling in food engineering. *Journal of Food Engineering*, *1140*(3), 279–291.
Huang, S. R., Yang, J. I., & Lee, Y. C. (2013). Interactions of heat and mass transfer in steam reheating of starchy foods. *Journal of Food Engineering*, *1140*(2), 174–182.
Jin, X., van Boxtel, A. J. B., & van der Sman, R. (2012). Anomalies in moisture transport during broccoli drying monitored by MRI? *Faraday Discussions*, *158*, 65.
Jin, X., van der Sman, R. G. M., & van Boxtel, A. J. B. (2011). Evaluation of the free volume theory to predict moisture transport and quality changes during broccoli drying. *Drying Technology*, *290*(16, SI), 1963–1971.
Kneifel, W., Paquin, P., Abert, T., & Richard, J. -P. (1991). Water-holding capacity of proteins with special regard to milk proteins and methodological aspects — A review. *Journal of Dairy Science*, *740*(7), 2027–2041.
Kristinsson, H. G., & Hultin, H. O. (2003). Role of pH and ionic strength on water relationships in washed minced chicken-breast muscle gels. *Journal of Food Science*, *680*(3), 917–922.
Lago, M., & Araujo, M. (2003). Threshold capillary pressure in capillaries with curved sides. *Physica A: Statistical Mechanics and its Applications*, *319*, 175–187.
Lantto, R., Puolanne, E., Kruus, K., Buchert, J., & Autio, K. (2007). Tyrosinase-aided protein cross-linking: Effects on gel formation of chicken breast myofibrils and texture and water-holding of chicken breast meat homogenate gels. *Journal of Agricultural and Food Chemistry*, *550*(4), 1248–1255.
Leksrisompong, P. N., Lanier, T. C., & Foegeding, E. A. (2012). Effects of heating rate and pH on fracture and water-holding properties of globular protein gels as explained by micro-phase separation. *Journal of Food Science*, *77*(2), E60–E67.
Lepetit, J. (1989). Deformation of collagenous, elastin and muscle fibers in raw meat in relation to anisotropy and length ratio. *Meat Science*, *260*(1), 47–66.
Lepetit, J. (2007). A theoretical approach of the relationships between collagen content, collagen cross-links and meat tenderness. *Meat Science*, *760*(1), 147–159.
Lepetit, J. (2008). Collagen contribution to meat toughness: Theoretical aspects. *Meat Science*, *800*(4), 960–967.
Lewis, G. J., & Purslow, P. P. (1990). Connective number differences in the strength of cooked meat across the muscle fibre direction due to test specimen size. *Meat Science*, *280*(3), 183–194.
Locker, R. H., & Daines, G. J. (1976). Transverse anisotropy in beef muscle. *Journal of the Science of Food and Agriculture*, *270*(2), 186–192.
Luikov, A. V. (1966). Application of irreversible thermodynamics methods to investigation of heat and mass transfer. *International Journal of Heat and Mass Transfer*, *90*(2), 139–152.
Mathlouthi, Mohamed (2001). Water content, water activity, water structure and the stability of foodstuffs. *Food Control*, *120*(7), 409–417.
Matsuyama, Akihiko, & Tanaka, Fumihiko (1990). Theory of solvation-induced reentrant phase separation in polymer solutions. *Physical Review Letters*, *650*(3), 341–344.
McKenna, Gregory B., & Horkay, Ferenc (1994). Effect of crosslinks on the thermodynamics of poly(vinyl alcohol) hydrogels. *Polymer*, *350*(26), 5737–5742.
Mercadé-Prieto, R., Falconer, R. J., Paterson, W. R., & Wilson, D. I. (2007). Swelling and dissolution of β-lactoglobulin gels in alkali. *Biomacromolecules*, *80*(2), 469–476.
Mir-Bel, J., Oria, R., & Salvador, M. L. (2009). Influence of the vacuum break conditions on oil uptake during potato post-frying cooling. *Journal of Food Engineering*, *950*(3), 416–422.
Mortensen, L. M., Frøst, M. B., Skibsted, L. H., & Risbo, J. (2012). Effect of time and temperature on sensory properties in low-temperature long-time sous-vide cooking of beef. *Journal of Culinary Science & Technology*, *100*(1), 75–90.
Murphy, R. Y., Johnson, E. R., Duncan, L. K., Clausen, E. C., Davis, M. D., & March, J. A. (2001). Heat transfer properties, moisture loss, product yield, and soluble proteins in chicken breast patties during air convection cooking. *Poultry Science*, *800*(4), 508–514.
Naveena, B. M., Mendiratta, S. K., & Anjaneyulu, A. S. R. (2004). Tenderization of buffalo meat using plant proteases from *Cucumis trigonus* rox (kachri) and *Zingiber officinale* roscoe (ginger rhizome). *Meat Science*, *680*(3), 363–369.
Ni, H., Datta, A. K., & Torrance, K. E. (1999). Moisture transport in intensive microwave heating of biomaterials: A multiphase porous media model. *International Journal of Heat and Mass Transfer*, *420*(8), 1501–1512.
Offer, G., Knight, P., Jeacocke, R., Almond, R., Cousins, T., Elsey, J., Parsons, N., Sharp, A., Starr, R., & Purslow, P. (1989). The structural basis of the water-holding, appearance and toughness of meat and meat products. *Food Microstructure*, *8*.
Offer, G., & Trinick, J. (1983). On the mechanism of water holding in meat: The swelling and shrinking of myofibrils. *Meat Science*, *80*(4), 245–281.
Oillic, S., Lemoine, E., Gros, J. B., & Kondjoyan, A. (2011). Kinetic analysis of cooking losses from beef and other animal muscles heated in a water bath effect of sample dimensions and prior freezing and ageing. *Meat Science*, *880*(3), 338–346.
Okuzono, Tohru, & Doi, Masao (2008). Effects of elasticity on drying processes of polymer solutions. *Physical Review E*, *770*(3), 030501.
Parker, J. C., Lenhard, R. J., & Kuppusamy, T. (1987). A parametric model for constitutive properties governing multiphase flow in porous media. *Water Resources Research*, *230*(4), 618–624.
Perré, Patrick, & Turner, Ian W. (1999). A 3-D version of transpore: A comprehensive heat and mass transfer computational model for simulating the drying of porous media. *International Journal of Heat and Mass Transfer*, *420*(24), 4501–4521.
Puolanne, E., & Halonen, M. (2010). Theoretical aspects of water-holding in meat. *Meat Science*, *860*(1), 151.
Puolanne, E., & Peltonen, J. (2013). The effects of high salt and low pH on the water-holding of meat. *Meat Science*, *930*(2), 167–170.
Quesada-Pérez, M., Maroto-Centeno, J. A., Forcada, J., & Hidalgo-Alvarez, R. (2011). Gel swelling theories: The classical formalism and recent approaches. *Soft Matter*, *70*(22), 10536–10547.
Quintard, M., & Whitaker, S. (1993). Transport in ordered and disordered porous media: Volume-averaged equations, closure problems, and comparison with experiment. *Chemical Engineering Science*, *480*(14), 2537–2564.
Rajkumar, V., Moreira, R., & Barrufet, M. (2003). Modeling the structural changes of tortilla chips during frying. *Journal of Food Engineering*, *600*(2), 167–175.
Rowe, R. W. D. (1981). Morphology of perimysial and endomysial connective number in skeletal muscle. *Tissue & Cell*, *130*(4), 681–690.
Schmidt, F. C., Carciofi, B. A. M., & Laurindo, J. B. (2008). Salting operational diagrams for chicken breast cuts: Hydration–dehydration. *Journal of Food Engineering*, *880*(1), 36–44.
Schmidt, F. C., Carciofi, B. A. M., & Laurindo, J. B. (2009). Application of diffusive and empirical models to hydration, dehydration and salt gain during osmotic treatment of chicken breast cuts. *Journal of Food Engineering*, *910*(4), 553–559.
Schreyer-Bennethum, Lynn (2012). Macroscopic flow potentials in swelling porous media. *Transport in Porous Media*, 1–22.
Skipnes, D., Johnsen, S. O., Skåra, T., Sivertsvik, M., & Lekang, O. (2011). Optimization of heat processing of farmed Atlantic cod (*Gadus morhua*) muscle with respect to cook loss, water holding capacity, color, and texture. *Journal of Aquatic Food Product Technology*, *200*(3), 331–340.
Skipnes, D., Van der Plancken, I., Van Loey, A., & Hendrickx, M. E. (2008). Kinetics of heat denaturation of proteins from farmed Atlantic cod (*Gadus morhua*). *Journal of Food Engineering*, *850*(1), 51–58.
Stanish, M. A., Schajer, G. S., & Kayihan, F. (2004). A mathematical model of drying for hygroscopic porous media. *AICHE Journal*, *320*(8), 1301–1311.
Stevenson, C. D., Dykstra, M. J., & Lanier, T. C. (2013). Capillary pressure as related to water holding in polyacrylamide and chicken protein gels. *Journal of Food Science*. http://dx.doi.org/10.1111/1750-3841.12036.
Stevenson, C. D., Liu, W., & Lanier, T. C. (2012). Rapid heating of Alaska Pollock and chicken breast myofibrillar protein gels as affecting water holding properties. *Journal of Agricultural and Food Chemistry*, *600*(40), 10111–10117.
Tanaka, H. (2012). Viscoelastic phase separation in soft matter and foods. *Faraday Discussions*, *158*.
Tornberg, E. (2005). Effects of heat on meat proteins — Implications on structure and quality of meat products. *Meat Science*, *700*(3), 493–508.

Vagenas, G. K., Marinos-Kouris, D., & Saravacos, G. D. (1990). An analysis of mass transfer in air-drying of foods. *Drying Technology*, *80*(2), 323–342.
van der Sman, R. G. M. (2007a). Moisture transport during cooking of meat: An analysis based on Flory–Rehner theory. *Meat Science*, *760*(4), 730–738.
van der Sman, R. G. M. (2007b). Soft condensed matter perspective on moisture transport in cooking meat. *AIChE Journal*, *530*(11), 2986–2995.
van der Sman, R. G. M. (2008). Prediction of enthalpy and thermal conductivity of frozen meat and fish products from composition data. *Journal of Food Engineering*, *840*(3), 400–412.
van der Sman, R. G. M. (2012a). Soft matter approaches to food structuring. *Advances in Colloid and Interface Science*, *176–177*, 18–30.
van der Sman, R. G. M. (2012b). Thermodynamics of meat proteins. *Food Hydrocolloids*, *270*(2), 529–535.
van der Sman, R. G. M. (2013). Prediction of the moisture sorption in ternary mixtures of biopolymer, disaccharides and water by the FVFH theory. *Food Hydrocolloids*, *32*(1), 186–194.
van der Sman, R. G. M., & Boer, E. (2005). Predicting the initial freezing point and water activity of meat products from composition data. *Journal of Food Engineering*, *660*(4), 469–475.
van der Sman, R. G. M., & Meinders, M. B. J. (2011). Prediction of the state diagram of starch water mixtures using the Flory–Huggins free volume theory. *Soft Matter*, *70*(2), 429–442.
van der Sman, R. G. M., & Meinders, M. B. J. (2013). Moisture diffusivity in food materials. *Food Chemistry*, *1380*(2–3), 1265–1274.
van der Sman, R. G. M., & van der Goot, A. J. (2009). The science of food structuring. *Soft Matter*, *50*(3), 501–510.
van der Sman, R. G. M., Voda, A., Khalloufi, S., & Paudel, E. (2013). Water holding capacity of rehydrated, freeze-dried vegetables. *Food Chemistry* (submitted for publication).
Waananen, K. M., Litchfield, J. B., & Okos, M. R. (1993). Classification of drying models for porous solids. *Drying Technology*, *110*(1), 1–40.
Wählby, Urban, & Skjöldebrand, Christina (2001). NIR-measurements of moisture changes in foods. *Journal of Food Engineering*, *470*(4), 303–312.
Wallach, R., Troygot, O., & Saguy, I. S. (2011). Modeling rehydration of porous food materials: II. The dual porosity approach. *Journal of Food Engineering*, *1050*(3), 416–421.
Wang, Xiao, & Hong, Wei (2010). Surface interactions between two like-charged polyelectrolyte gels. *Physical Review E*, *810*(4), 041803.
Weerts, A. H., Lian, G., & Martin, D. R. (2004). Modeling the hydration of foodstuffs: Temperature effects. *AIChE Journal*, *490*(5), 1334–1339.
Weerts, A. H., Lian, G., & Martin, D. (2006). Modeling rehydration of porous biomaterials: Anisotropy effects. *Journal of Food Science*, *680*(3), 937–942.
Whitaker, S. (1983). Drying granular porous media — Theory and experiment. *Drying Technology*, *10*(1), 3–33.
Wolfe, Joe, Bryant, Gary, & Koster, Karen L. (2002). What is unfreezable water, how unfreezable is it and how much is there? *CryoLetters*, *230*(3), 157–166.
Zhang, J., & Datta, A. K. (2004). Some considerations in modeling of moisture transport in heating of hygroscopic materials. *Drying Technology*, *220*(8), 1983–2008.
Zhang, J., & Datta, A. K. (2006). Mathematical modeling of bread baking process. *Journal of Food Engineering*, *750*(1), 78–89.